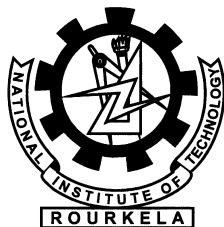


Comparative Analysis of Hashing Schemes for Iris Identification using Local Features

Ravi Kumar



Department of Computer Science and Engineering
National Institute of Technology Rourkela
Rourkela-769 008, Odisha, India

Comparative Analysis of Hashing Schemes for Iris Identification using Local Features

*Thesis submitted in partial fulfillment
of the requirements for the degree of*

Master of Technology
(Research)

in

Computer Science and Engineering

by

Ravi Kumar
(Roll: 611CS104)

under the guidance of

Prof. Banshidhar Majhi
NIT Rourkela



Department of Computer Science and Engineering
National Institute of Technology Rourkela
Rourkela-769 008, Odisha, India



Department of Computer Science and Engineering
National Institute of Technology Rourkela
Rourkela-769 008, Odisha, India.

January 30, 2014

Certificate

This is to certify that the work in the thesis entitled *Comparative Analysis of Hashing Schemes for Iris Identification using Local Features* by *Ravi Kumar* (roll number 611CS104), is a record of an original research work carried out under my supervision and guidance in partial fulfillment of the requirements for the award of the degree of Master of Technology (Research) in Computer Science and Engineering. Neither this thesis nor any part of it has been submitted for any degree or academic award elsewhere.

Banshidhar Majhi
Professor
CSE department of NIT Rourkela

Acknowledgment

I owe deep gratitude to the ones who have contributed greatly in completion of this thesis.

Foremost, I would like to express my sincere gratitude to my advisor, Prof. Ban-shidhar Majhi for providing me a platform to work on challenging area of biometrics. His profound insights and attention to details have been true inspirations to my research.

I am very much indebted to Prof. Bidyadhar Subudhi, Prof. Sanjay Kumar Jena, and Prof. Dipti Patra for providing insightful comments at different stages of thesis that were indeed thought provoking. My special thanks goes to Prof. Pankaj Kumar Sa and Prof. Ratnakar Dash for contributing towards enhancing the quality of the work in shaping this thesis.

I would like to thank all my friends and lab-mates for their encouragement and understanding. Their help can never be penned with words.

Most importantly, none of this would have been possible without the love and patience of my family. My family to whom this dissertation is dedicated to, has been a constant source of love, concern, support and strength all these years. I would like to express my heart-felt gratitude to them.

Ravi Kumar

Abstract

Iris is one of the most reliable biometric trait due to its stability and randomness. Traditional recognition systems transform the iris to polar coordinates and perform well for co-operative databases. However, the problem aggravates to manifold for recognizing non-cooperative irises. In addition, the transformation of iris to polar domain introduces aliasing effect. In this thesis, *Noise Independent Annular Iris* is used for feature extraction. Global feature extraction approaches are rendered as unsuitable for annular iris due to change in scale as they could not achieve invariance to transformation and illumination. On the contrary, local features are invariant to image scaling, rotation, and partially invariant to change in illumination and viewpoint. To extract local features, *Scale Invariant Feature Transform* (SIFT) has been applied to annular iris. However, SIFT is computationally expensive for recognition due to higher dimensional descriptor. Thus, a keypoint descriptor called *Speeded Up Robust Features* (SURF) is applied to mark performance improvement in terms of time as well as accuracy. At last, a recently developed *Binary Robust Invariant Scalable Keypoints* (BRISK) is applied. BRISK performs at a dramatically lower computational cost than SIFT and SURF.

For identification, retrieval time plays a significant role in addition to accuracy. Traditional indexing approaches cannot be applied to biometrics as data are unstructured. In this thesis, two novel approaches has been applied for indexing iris database. In the first approach, indexing is done using *Geometric Hashing* of local feature keypoints. This approach achieves invariance to similarity transformations, illumination, and occlusion and performs with a good accuracy for cooperative as well as non-cooperative databases, but it takes larger time for recognition. In the second approach, enhanced geometric hashing is applied using local keypoint descriptors of annular iris for different databases. Comparative analysis shows that enhanced geometric hashing is more accurate and faster than traditional geometric hashing.

Keywords: Keypoint, geometric hashing, difference of Gaussian, descriptor, and feature vector.

Contents

Certificate	ii
Acknowledgement	iii
Abstract	iv
List of Figures	vii
List of Tables	x
1 Introduction	1
1.1 Iris Biometrics	5
1.2 Various Performance Measures	7
1.3 Iris Databases used in the Research	8
1.4 Literature Review	10
1.4.1 Feature Representation	11
1.4.2 Identification	11
1.5 Motivation	12
1.6 Thesis Organization	13
2 Local Features for Iris	15
2.1 Scale Invariant Feature Transform (SIFT)	16
2.1.1 Keypoint Detection	16
2.1.2 Keypoint Descriptor	19
2.1.3 Keypoint Pairing	20
2.2 Speeded Up Robust Features (SURF)	20
2.2.1 Detection of Keypoints	21
2.2.2 Keypoint Descriptor	24
2.2.3 Keypoint Pairing	26

2.3	Binary Robust Invariant Scalable Keypoints (BRISK)	27
2.3.1	Keypoint Detection	27
2.3.2	Keypoint Description	28
2.3.3	Descriptor Matching	30
2.4	Summary	32
3	Iris Identification	33
3.1	Indexing based on Geometric Hashing	34
3.1.1	Indexing	34
3.1.2	Iris Retrieval	37
3.2	Indexing based on Enhanced Geometric Hashing	38
3.2.1	Preprocessing	38
3.2.2	Hash Table Generation	40
3.2.3	Searching	40
3.3	Comparative analysis of Geometric Hashing and Enhanced Geometric Hashing	41
3.3.1	Comparative analysis using SIFT	42
3.3.2	Comparative analysis using SURF	44
3.3.3	Comparative analysis using BRISK	47
3.4	Summary	49
4	Conclusions and Future Work	50
	Bibliography	52
	Dissemination	56

List of Figures

1.1	Various forms of authentication. Left: Traditional methods of authentication using token based and knowledge based approaches. Right: Use of biometrics to claim identity.	2
1.2	Different modules of biometrics system.	3
1.3	Different modes of biometric recognition	4
1.4	A sample image from CASIA database [1] that depicts the anatomy of human eye [2].	6
1.5	Preprocessing of iris image: (a) Input iris image, (b) Geometrical representation of sectors on iris circles, (c) Noise independent annular iris image after preprocessing [3].	9
2.1	Gaussian blurred iris images (left), and Gaussian images are subtracted to produce DoG images (right).	18
2.2	Maxima and minima of DoG images are obtained by comparing a pixel to 26 neighbors in $3 \times 3 \times 3$ regions [4]	19
2.3	Keypoint detection on an annular iris image using SIFT (a) Detected keypoints after removing noise and edge responses, (b) Scale and direction of orientation (indicated by arrows).	19
2.4	Window is taken relative to direction of dominant orientation. This window is weighted by a Gaussian and histogram is obtained for 4×4 regions [2].	20
2.5	Integral images are used to calculate the sum of intensities inside a rectangular region of any size [2].	21

2.6	Left to right: discrete Gaussian second order derivative in y and xy direction. Approximation for the second order Gaussian partial derivative in y -direction (D_{yy}) and xy -direction (D_{xy}) [5].	22
2.7	Use of integral images for upscaling filter masks [6].	23
2.8	Filters D_{yy} (top) and D_{xy} (bottom) for two successive filter sizes (9×9 and 15×15) [6].	24
2.9	SURF detected keypoints on the annular iris image.	24
2.10	Orientation assignment by taking a sliding window of size $\frac{\pi}{3}$ indicated by shaded region [6].	25
2.11	An oriented window with 4×4 sub-regions is taken in the direction of orientation. For each sub-region wavelet responses are obtained [6].	26
2.12	Scale-space interest point detection: a keypoint is identified at octave c_i by analyzing the 8 neighboring saliency scores in c_i as well as in the corresponding scores-patches in the immediately-neighboring layers above and below [7].	28
2.13	The BRISK sampling pattern with $N_l = 60$ points: the small blue circles denote the sampling locations; the bigger, red dashed circles are drawn at a radius σ corresponding to the standard deviation of the Gaussian kernel used to smooth the intensity values at the sampling points [7].	29
2.14	BRISK interest point matching on two annular iris images.	31
3.1	Block diagram for geometric hashing based indexing approach [3].	34
3.2	Similarity transformation: (a) Two dimensional representation of detected keypoints from annular iris image, (b) Keypoints after similarity transformation for basis pair $k_1 k_2$, (c) Keypoints after similarity transformation of possible basis pairs, and (d) Keypoints after rehashing.	36
3.3	(a) Two dimensional representation of detected keypoints from annular iris image, (b) Keypoints after mean centering.	39
3.4	(a) Keypoints after rotation with respect to principal components, (b) Keypoints after normalization.	40

3.5	CMC curve for geometric hashing and enhanced geometric hashing using SIFT on different iris databases, (a) BATH, (b) CASIA, (c) IITK, and (d) UBIRIS.	44
3.6	CMC curve for geometric hashing and enhanced geometric hashing using SURF on different iris databases, (a) BATH, (b) CASIA, (c) IITK, and (d) UBIRIS.	45
3.7	CMC curve for geometric hashing and enhanced geometric hashing using BRISK on different iris databases, (a) BATH, (b) CASIA, (c) IITK, and (d) UBIRIS.	49

List of Tables

1.1	Images taken from different iris databases for testing.	10
2.1	Comparative study of SIFT, SURF, and BRISK based on feature extraction and matching techniques.	31
2.2	Comparative of SIFT, SURF, and BRISK for a single CASIA iris image.	32
3.1	The time taken in binning of a single image for different databases.	42
3.2	Identification probabilities at various ranks for geometric hashing (GH) and enhanced geometric hashing (EGH) using SIFT keypoints.	43
3.3	Identification probabilities at various ranks for geometric hashing (GH) and enhanced geometric hashing (EGH) using SURF keypoints.	46
3.4	Identification probabilities at various ranks for geometric hashing (GH) and enhanced geometric hashing (EGH) using BRISK keypoints.	48

Chapter 1

Introduction

Personal identification is a fundamental activity in our society. Traditional authentication systems are based on (a) token based systems: where authentication for accessing protected resources is done using identity (ID) cards, smart cards, etc., (b) knowledge-based systems: where identity is claimed using secret keys like username and password associated with it. Some systems use a combination of token based and knowledge-based approaches. However, there are various disadvantages inherent to traditional means of authentication. The problem with token based systems is that the evidence could be stolen, lost or misplaced. The drawback of knowledge-based approaches is that it is difficult to remember passwords or PIN (Personal Identification Number) and easily recallable passwords can be guessed by intruders. Thus, even the combination of knowledge and token based systems could not fulfill security requirements [8]. This identification is made possible by the emergence of the new concept of biometrics. Biometrics identification provides a trustable solution to the problems faced by conventional authentication approaches. It is inherently more reliable and capable compared with conventional approaches. Biometric identifiers for personal authentication reduce or eliminate reliance on tokens, PINs, and passwords. Various modes of authentication are shown in Figure 1.1. It can be integrated into any application that requires security, access control, and identification or verification of people [9].

Biometrics is the science of establishing the identity of an individual based on the physical or behavioral attributes of the person. Physiological biometrics is based on measurements and data derived from direct measurement of a part of the human

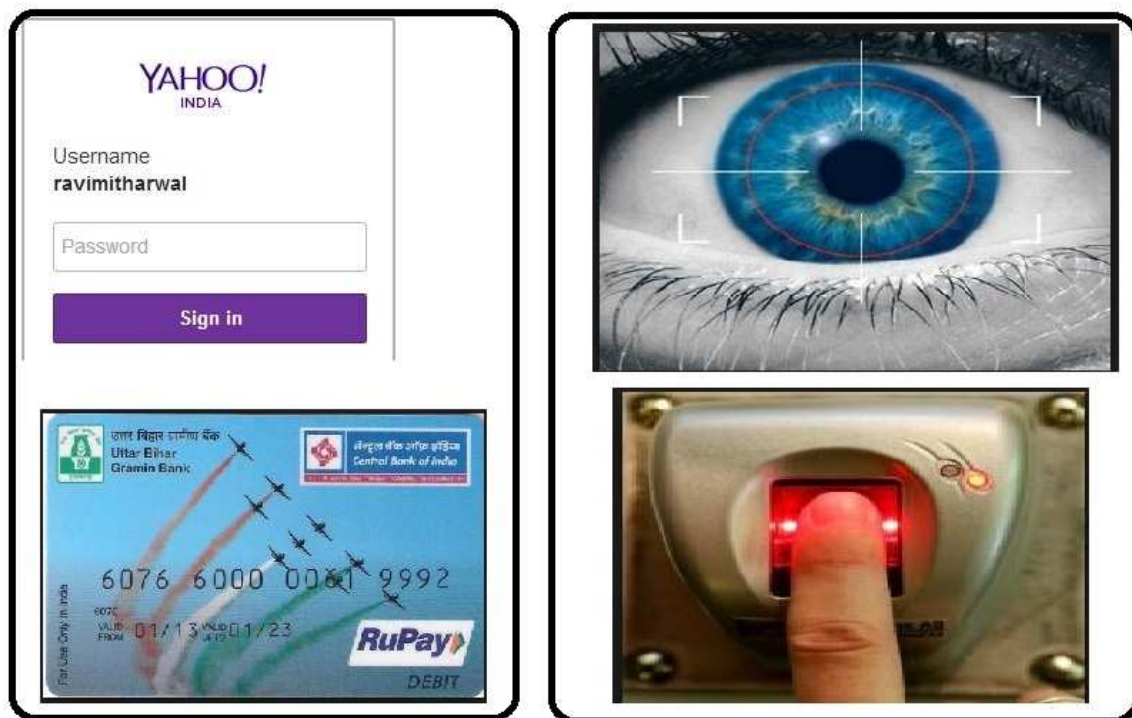


Figure 1.1: Various forms of authentication. Left: Traditional methods of authentication using token based and knowledge based approaches. Right: Use of biometrics to claim identity.

body. Iris, fingerprint, palmprint, and face recognition are leading physiological biometrics. Behavioral characteristics, on the other hand, are based upon an action taken by a person. Behavioral biometrics is based on measurements and data derived from an action, and indirectly measure characteristics of the human body. Signature, voice recognition, and keystroke dynamics are leading behavioral biometric technologies. The primary advantage of biometrics over token based and knowledge-based approaches is that, it cannot be misplaced, forgotten or stolen. The characteristics are distinct and can identify authorized persons. It is very difficult to spoof biometric systems as the person to be authenticated needs to be physically present. The use of biometric system for recognition purposes requires following characteristics.

- *Distinctiveness*: Any two persons should be sufficiently different in terms of the attributes.
- *Universality* : Each person should possess the attributes. The attribute must be

one that is universal and seldom lost to accident or disease.

- *Collectability* : The attributes should be measured quantitatively.
- *Permanence* : The attributes should be sufficiently invariant over a period of time.
- *Reducibility* : The captured data should be capable of being reduced to a file which is easy to handle.
- *Inimitable* : The attribute must be irreproducible by other means. The less reproducible the attribute, the more likely it will be authoritative.
- *Privacy* : The process should not violate the privacy of the person.

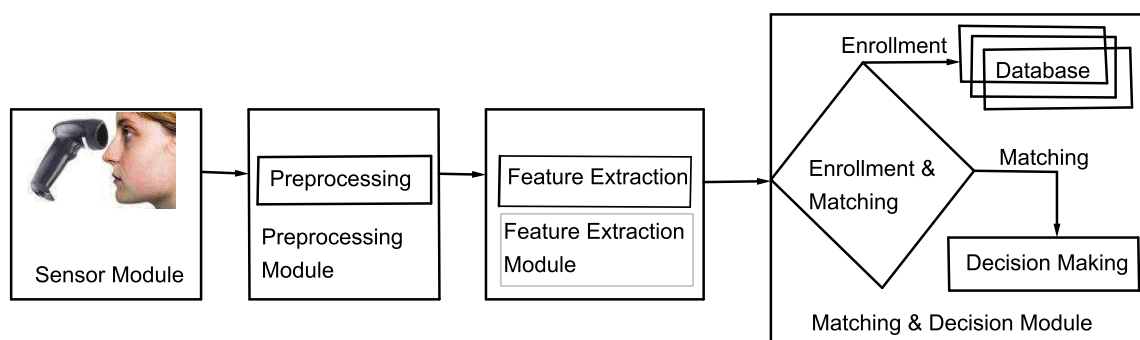
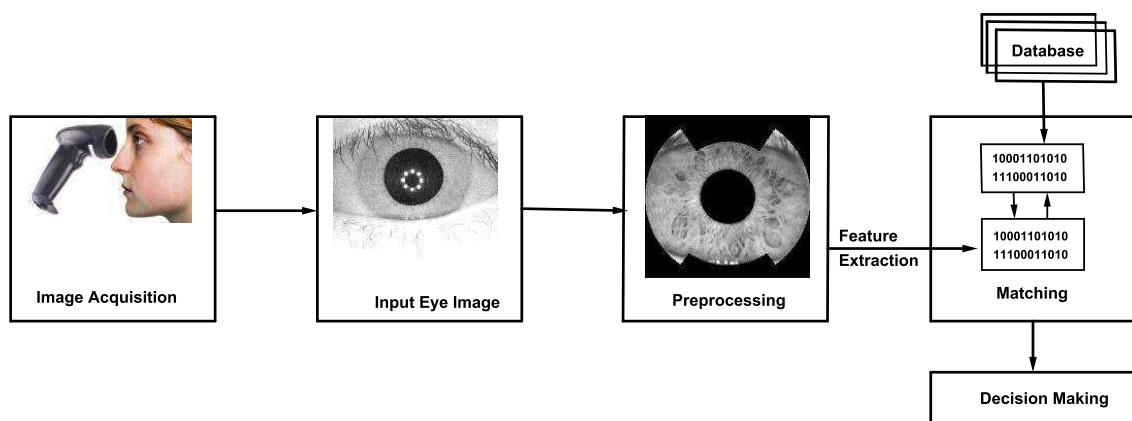


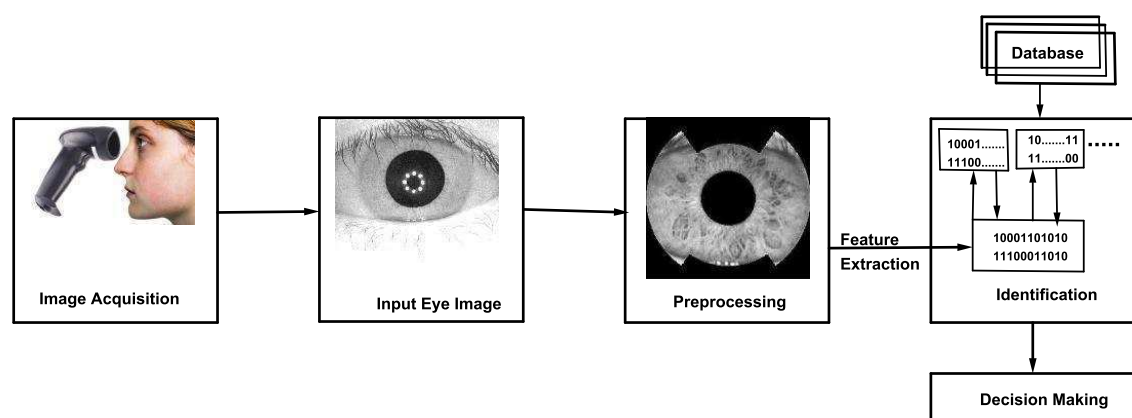
Figure 1.2: Different modules of biometrics system.

A biometric system is essentially a pattern recognition system that operates in three steps. First, acquire biometric data from an individual. Second, extract a feature set from the acquired data. Third, authentication of an individual based on the result of comparison of the feature set against the template set in the database [10]. The modules involved in the biometric system are given in Figure 1.2. An important issue to be considered while designing a biometric system is how a person is recognized. Based on the application context a biometric system operates in two different modes [11]. In *verification* mode, the system validates a candidate's identity by comparing the captured biometric data with his own biometric template stored in the system database. In such a system, a person who desires to be recognized claims an identity,

usually via a PIN, a user name, a smart card, etc. The system conducts one to one comparison to know whether the identity claimed by an individual is genuine or not. The diagrammatic representation of the verification system is given in Figure 1.3(a). In *identification* mode, the system searches the entire database to find the identity of a person. Therefore, the system conducts a one-to-many comparisons to establish a candidate's identity. The diagrammatic representation of identification is given in Figure 1.3 (b). Applications of biometrics include sharing networked computer resources, granting access to nuclear facilities, performing remote financial transactions or boarding a commercial flight.



(a) Verification mode (one to one comparison)



(b) Identification mode (one to many comparisons)

Figure 1.3: Different modes of biometric recognition

Biometrics such as signatures, fingerprints, voice, and retinal blood vessel patterns all have significant drawbacks. Although signatures are cheap and easy to obtain and

store, they are impossible to identify automatically with assurance, and can be easily forged. Electronically recorded voice is susceptible to changes in a person's voice, and they can be counterfeited. Fingerprints or palmprints required physical contact, and they also can be counterfeited and marred by artifacts. Human iris, on the other hand, as an internal organ of the eye and as well protected from the external environment. It is easily visible from one meter distance and is a perfect biometric trait for an identification system with the ease of speed, reliability, and automation. In this thesis, we are going to experiment, implement, and most importantly, look into the theory behind an Iris Recognition System, which is related to the personal identification by an automated biometric system.

1.1 Iris Biometrics

Reliability is particularly dependent on the ability to acquire unique features that can be captured in an invariant fashion over change in time [12]. Although, each biometrics has several strengths and limitations, and their deployment is dependent upon the application scenario. For example, fingerprint features remain unique over passage of time while face can vary significantly with change in time. In addition to this, as few constraints as possible should be imposed on the user giving biometric data. Fingerprint acquisition is invasive as it requires the user to make physical contact with the sensor. Among various available biometric traits, iris plays a significant role to provide a promising solution to authenticate an individual using unique texture patterns [13]. Taking reliability and invasiveness into consideration, iris is proven to be the most efficient technique. From the point of view of reliability, the spatial patterns are unique to each individual in the entire human population. From the point of view of invasiveness, iris is protected internal organ whose random texture is stable throughout life. It can serve as a kind of living password that one need not to remember but always carries along. The purpose is to provide the real-time high assurance recognition of an individual's identity by mathematical analysis of the random patterns that are visible within the iris.

Iris is the most promising and significant feature in the eye image as shown in

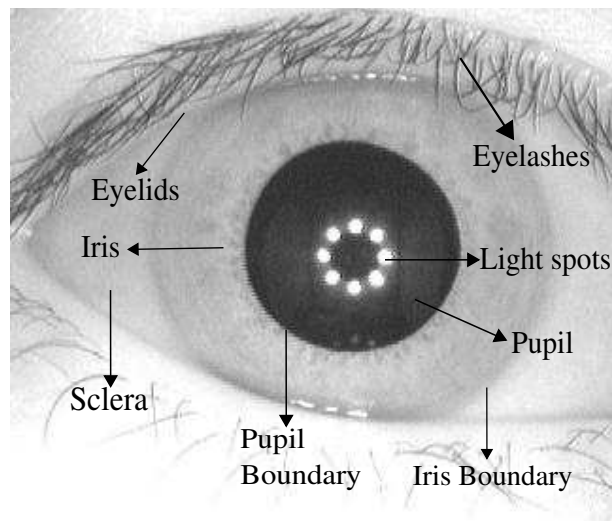


Figure 1.4: A sample image from CASIA database [1] that depicts the anatomy of human eye [2].

Figure 1.4. The iris is in the form of circular ring that contains many interlacing minute characteristics such as freckles, coronas, stripes, furrows, crypts and so on. These minute patterns in the iris are unique to everyone and are not invasive to their users. Inside the iris, there is a central dark circle known as a pupil. The circumference of pupil and iris is known as pupil and iris boundary respectively. Sclera is the white portion, a tough and leather like tissue surrounding the iris. Apart from these features, eyeball is covered by upper and lower eyelids. The upper eyelid is a stretchable membrane that can form a cover over the eye. It has a great freedom of motion, ranging from wide open to close. The lower eyelid, on the other hand, has a smaller degree of motion, which is caused by deformation due to eyeball [14]. An eyelash is the hairs that grows at the edge of the eyelid and protects the eye from dust.

Image processing techniques are used to extract the iris from the acquired image of an eye, and generate a biometric template, which can be stored in the database. This biometric template contains a mathematical representation of unique texture information stored in the iris, and allows comparisons to be made between individuals. When a person wishes to be identified by an iris recognition system, his eye is first photographed, and then a template is created for iris region. This template is then compared with all the templates stored in a database. The person is identified if a

matching template is found, else the person remains unidentified.

1.2 Various Performance Measures

The matching between two passwords is obtained by finding a perfect match between two alphanumeric strings. However, biometrics rarely compares exactly same templates. There is a difference between two templates due to occlusion, change in characteristics with respect to aging, change in acquisition conditions, etc. Thus, the feature sets originating from same individual may look different. When two different biometric templates originating from same individual are not same, it is known as *intra-class* variations. However, variations that occur between templates originating from two different individuals are known as *inter-class* variations [15]. When the two biometric templates are compared to find intra-class variations then such scores are known as similarity/genuine scores. The score that lies below threshold (τ) results in false rejection. However, when two biometric traits are compared to find inter-class similarity, then scores are known as imposter scores. The scores that exceed a pre-defined threshold value, results in false acceptance. The commonly used measures to evaluate the performance of the biometric system are:

- *False Rejection Rate (FRR)*: A false reject occurs when an individual is not matched correctly to his/her own existing biometric template. FRR is the frequency of rejections relative to people who should be correctly verified.
- *False Acceptance Rate (FAR)*: A false accept occurs when an individual is incorrectly matched to another individual's existing biometric template. FAR is the frequency of fraudulent access to imposters claiming identity [16].
- *Equal Error Rate (EER)*: ERR is the point where FAR is equal to FRR. In general, the lower the equal error rate value, the higher the accuracy of the biometric system.
- *Genuine Acceptance Rate (GAR)*: GAR is the fraction of genuine scores exceeding the threshold τ . It is defined as

$$GAR = 1 - FRR \tag{1.1}$$

- *Cumulative Match Characteristic (CMC) Curve*: The rank- t_k indicates the number of correct identities that occur in top t_k matches. Let q_k denote the number of elements of a query set present in top t_k and q_n denote total elements of query set then the probability of identification is given by $I = q_k/q_n$. CMC curve represents the probability of identification I at various top t_k ranks [17].

1.3 Iris Databases used in the Research

To measure the performance of automated iris biometric system, extensive experiments are carried out at various levels. This section discusses in detail about the databases used in experiments. Experimental results are obtained on various available datasets such as UBIRIS version 1 [18], BATH [19], CASIA version 3 [1], and Indian Institute of Technology Kanpur (IITK) [20]. These databases take all possible factors into consideration like rotation, illumination, scaling, and noise. These databases are classified into cooperative and non-cooperative categories based on the restrictions imposed on the user while capturing images.

- *Cooperative Database*: These databases are acquired under ideal conditions with less imposition on the user. Such databases consider less noise factors during image acquisition. BATH and CASIA version 3 fall under this category.
- *Non-cooperative Database*: Non-cooperative databases are collected to bring noisy factors into consideration with less constrained image acquisition environment. UBIRIS version 1 and few images of IITK database are considered under this category.

The image acquisition system captures iris as a larger portion of image that also contains data from immediately surrounding eye region [21] as shown in Figure 1.5(a). Thus, prior to performing feature extraction it is necessary to localize only that portion of the image that contains purely iris. Specially, it is important to localize the region between inner pupil and outer iris boundary. The iris is occluded by eyelids, hence the portion below the upper eyelid and above the lower eyelid should be considered for feature extraction. In a normal gaze, the edge of the upper eyelid intersects

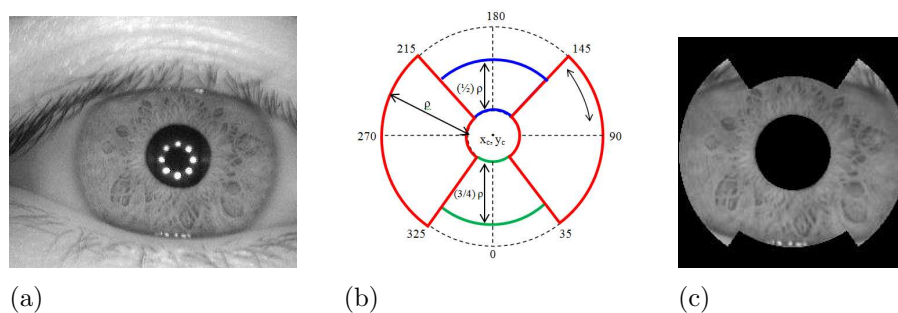


Figure 1.5: Preprocessing of iris image: (a) Input iris image, (b) Geometrical representation of sectors on iris circles, (c) Noise independent annular iris image after preprocessing [3].

the sclera and approximately half of the upper iris circle whereas, lower eyelid covers one-fourth of the lower iris circle. However, the left and the right regions are independent of such occlusions. Depending upon their degree of motion, upper eyelid adds more noise as compared to lower eyelid. It has been observed that, for the range of angular values θ , the regions that are not occluded due to eyelids are of range $[35^\circ, 145^\circ]$ and $[215^\circ, 325^\circ]$. For the upper and lower regions, only partial values of iris radius are taken from a sector. This generates a fixed size mask to remove eyelids from annular iris image. Figure 1.5 (b) shows the geometrical representation of sectors on annular iris circle where region underlying solid arcs are taken into consideration. The ratios $r_i/2$ and $3r_i/4$ are chosen depending on the degree of movement and occlusion of two eyelids. The noise independent annular iris image is complimentary to aliasing that occurs due to dimensionless polar coordinate conversion. The resultant preprocessed image is shown in Figure 1.5 (c). In this thesis, sector based annular iris databases are used for experiments. These databases are provided by H. Mehrotra [3].

The experiments performed in this thesis use only a limited number of images from different iris databases because at the time of identification, traditional geometric hashing technique takes larger time. Iris images taken from different iris databases for testing are shown in Table 1.1.

Table 1.1: Images taken from different iris databases for testing.

Iris Database	Database Size	Query Images
BATH	800	50
CASIA	650	100
IITK	600	50
UBIRIS	850	200

1.4 Literature Review

The first automated biometrics system was proposed in 1987 by Flom and Safir [22]. The authors have suggested highly controlled conditions that includes headrest, an image to direct gaze and manual operator. To account for variation in size of iris due to expansion and contraction of pupil, the illumination has been changed to make pupil of predetermined size. The first operational iris biometric system has been developed at University of Cambridge by Daugman [23]. The digital images of eye has been captured using near-infrared light source so that illumination could be controlled, that remains unaffected to users. The image acquisition system is highly robust where the algorithm maximizes the spectral power by adjusting focus of the system. The next step is to find the iris in the image that uses deformable templates. A deformable template is trained with some parameters and shape of the eye to guide the detection process [24]. Daugman presumed iris and pupil boundaries to be circular. After iris segmentation, the next step is to describe features of iris for comparison. The first difficulty lies in iris comparison is that, all iris images are not of same size. The iris representation should be invariant to change in size, scale, orientation, etc. The distance between camera and eye affects the size of iris in an image. The iris pattern undergoes linear deformation due to change in illumination that causes pupil to dilate or contract and change in orientation of iris due to head tilt, camera position, movement of eyeball, etc. Daugman has addressed this problem by mapping iris into dimensionless polar coordinate system [25]. The normalized iris image is further used to extract phase information using 2D Gabor filters. The similarity between two iris representations generates the matching score. This section discusses in detail about work done in two most significant areas like feature extraction and identification.

1.4.1 Feature Representation

Several approaches have been developed for mathematical analysis of random texture patterns that are visible within the eye. Daugman has used Gabor filter to produce binary representation of iris [13]. Gaussian filter is used for texture representation in [26]. The gradient vector field of an iris image is convolved with a Gaussian filter, yielding a local orientation at each pixel from normalized iris image. D. G. Lowe [4] proposed a method for extracting distinctive unvarying features from images that can be used to perform reliable matching between different views of an object or scene. These features are unvarying to image scale and rotation to provide robust matching across a substantial range of affine distortion, change in 3D viewpoint, addition of noise, and change in illumination. The features are highly distinctive, in the sense that a single feature can correctly be matched with high probability against a large database of features from many images. Modified Log-Gabor filters are used [27] because Log-Gabor filters are strictly bandpass filters. Discrete Cosine Transform (DCT) is used for feature extraction in [28]. It is applied to rectangular patches rotated at 45 degrees from radial axis. The dimensionality of feature set is reduced by keeping three most discriminating binarized DCT coefficients. H. Bay *et al.* [5] proposed a novel scale and rotation invariant detector and descriptor, coined SURF. It outperforms previously proposed schemes with respect to repeatability, distinctiveness, and robustness, yet can be computed and compared much faster. F. Fernandez *et al.* [29] used SIFT for recognition using iris images. S. Leutenegger *et al.* [7] proposed BRISK and computational cost is lower than SURF, with high quality performance .

1.4.2 Identification

Iris based identification needs more attention because existing state-of-the-art shows that very few contributions have been made in this direction. There already exist few indexing schemes to partition the biometric database. H. J. Wolfson *et al.* [30] proposed geometric hashing, a technique originally developed in computer vision for matching geometric features. Matching is possible even when the recognizable database objects have undergone transformations or when only partial information

is present. Indexing hand geometry database using pyramid technique has been proposed in [31]. An iris indexing technique has been proposed in [32], based on the iris color for noisy iris images. The performance measures shows the effectiveness of iris color for indexing very large database. H. Mehrotra *et al.* [3] proposed robust iris indexing scheme using geometric hashing of SIFT keypoints. The proposed scheme considers sectional descriptors as well as relative spatial configuration for claiming identity. To overcome the effect of non-uniform illumination and partial occlusion due to eyelids, sectional features are extracted from noise independent annular iris image using the SIFT. Jayaraman *et al.* [33] proposed an enhanced geometric hashing. Unlike the available geometrical hashing, the proposed technique needs less time and memory and has uniform index distribution on the hash space without using rehashing.

1.5 Motivation

The features from iris image extracted using global transforms [21,25,28,34,35], fail to work under change in rotation, scaling, illumination, and viewpoint of two images [36]. The area underlying annular iris image changes due to illumination hence global transforms are not suitable for matching two iris images of variable size. Therefore, local feature descriptors are required that are invariant to change in scale, rotation, occlusion, and viewpoint of two iris images. During identification, the number of false acceptance grows geometrically with the increase in the size of the database. If FAR and FRR indicate the false accept and reject rates during verification, then rates of false accept (FAR_N) and reject (FRR_N) in the identification mode for database of size N are given by [31]

$$\begin{aligned}
 FAR_N &= 1 - (1 - FAR)^N \approx N \times FAR \\
 FRR_N &= FRR \\
 \text{Then, total number of False Acceptance} &= N \times (FAR_N) \\
 &\approx N^2 \times FAR
 \end{aligned} \tag{1.2}$$

There are two approaches to reduce error rates during identification. First is by reducing FAR of matching algorithm and second is by reducing search time during

identification. The FAR is limited by performance of an algorithm and cannot be reduced significantly. Thus, accuracy and speed of a biometric identification system can be improved by reducing the number of templates compared. The effect of reducing the search space during identification is given by mathematical formulation. Suppose the entire search space is reduced by a fraction F . Thus, the resultant FAR and FRR after search space reduction is given by

$$\begin{aligned} FAR_{N \times F} &= 1 - (1 - FAR)^{N \times F} \approx N \times F \times FAR \\ FRR_{N \times F} &= FRR \end{aligned} \tag{1.3}$$

This minimizes the number of records against which search has to be performed, which in turn reduces FAR during identification. Most of the time a hashing technique is used to reduce retrieval time. In iris biometrics the database is a collection of images and for identification content based image retrieval is required. For traditional hashing schemes data should be structured but images are unstructured. Therefore, traditional hashing techniques cannot work in the iris recognition. An efficient classification, clustering or indexing scheme is required to reduce the search space during identification [37, 38]. There already exist few indexing schemes to partition the biometric database. Based on the current research directions from the literature, investigations have been made in this thesis to propose a comparative analysis of indexing schemes for iris identification using local keypoint extraction.

1.6 Thesis Organization

The rest of the thesis is organized as follows.

Chapter 2 presents local features for iris. To extract robust attributes, local features around interest points known as *keypoints* are obtained and compared to find the similarity between the images. The most valuable property of a keypoint detector is its repeatability, i.e., whether it reliably finds the same interest points under different viewing conditions [5]. To extract features around keypoints the neighbourhood of every detected point is represented by a feature vector (descriptor). In the proposed work, three well known keypoint descriptors SIFT, SURF, and BRISK has

been applied to iris to extract features robust to transformations, illumination and partial occlusions.

The techniques presented in **Chapter 3** are used for indexing existing biometric databases. In this chapter two approaches are compared for search space reduction. In the first section, geometric hashing approach is used which allows for retrieval of model images that differ from query image by some kind of similarity transformation and occlusion. In the second section, enhanced geometric hashing is used and this is more effective to similarity transformation and occlusion than traditional geometric hashing. The third section presents a comparative analysis of hashing schemes for iris identification using local features.

Finally **Chapter 4** presents the concluding remarks, with scope for further research work.

Chapter 2

Local Features for Iris

Feature extraction involves simplifying the amount of information required to describe an input image. The purpose is recognition of an individual identity by mathematical analysis of the random patterns that are visible within the iris. There already exists several global feature extraction techniques for iris [39, 40]. The main drawback of global feature extraction techniques is their failure to extract relevant features, which do not vary with significant variations in pose, illumination, and viewpoint of an individual. Local features are invariant to image scaling, rotation, and partially unvarying to change in illumination and viewpoint. These local features have the capability to perform well under partial occlusion. In order to extract local features from iris, interest points, known as *keypoints*, are detected where there can be a corner, an isolated point of local intensity maximum or minimum, line endings, or a point on a curve where the curvature is locally maximum. Around the neighborhood of every detected keypoint, a descriptor is computed that represents the feature vector. This descriptor should be robust to noise, detection displacements, and geometric and photometric deformations [6].

In this thesis, local features are extracted from annular iris images. As discussed earlier, the reason behind considering annular iris is to overcome aliasing errors due to polar transformation. To mark an improvement in terms of time and accuracy, landmark keypoint descriptors have been applied to iris. The novel keypoint descriptor called *Scale Invariant Feature Transform* (SIFT) has been applied to iris [4]. SIFT performs excellent for various transformations as well as occlusion due to high dimensional descriptor. The dimension of the descriptor has a direct impact on the

recognition time. Therefore, lower dimensional features are desirable for fast keypoint matching. However, lower dimensional feature vectors are in general less distinctive than their high dimensional counterparts. *Speeded Up Robust Features* (SURF) [5] uses a faster keypoint detection scheme with reduced dimensional descriptor. SURF has been used for machine vision applications like camera calibration and object tracking [5]. Due to inherent advantages of SURF, it has been applied to iris biometrics for efficient recognition. A comprehensive evaluation on benchmark datasets reveals that *Binary Robust Invariant Scalable Keypoints* (BRISK) [7] is an adaptive feature extractor with a high-performance ratio at a dramatically lower computational cost. The key to speed lies in the application of a novel scale space *Features from Accelerated Segment Test* (FAST)-based detector [41] in combination with the bit-string descriptor. This descriptor vector assembled from intensity comparisons are retrieved by sampling of each keypoint neighborhood. This chapter discusses in detail about above mentioned three keypoint descriptors and their applicability to iris.

2.1 Scale Invariant Feature Transform (SIFT)

The SIFT technique provides a stable set of features while being less sensitive to local image distortions. Local features from an image are computed using a cascade filtering approach that minimizes the feature extraction cost by applying more expensive operations at locations that pass an initial test. Keypoints are detected using the Difference of Gaussian (DoG) images. During the feature extraction process local image gradients are measured at selected scale in region around each keypoint to form a descriptor vector. Detailed description of steps outlined above are given in the following subsections.

2.1.1 Keypoint Detection

The first step is to find potential keypoints that are invariant to scale and orientation. For each detected keypoint a detailed model is fit to determine location and scale. The orientation is assigned to each location based on image gradients. The steps for keypoint detection are as follows.

Detection of Scale Space Extrema

The main idea behind scale space extrema detection is to identify stable features from the iris texture that remains invariant to change in scale and viewpoint. This technique has been implemented efficiently by using the DoG image to identify the potential interest points [4]. The DoG $D(x, y, \sigma)$ of an iris image I is as,

$$D(x, y, \sigma) = L(x, y, K\sigma) - L(x, y, \sigma) \quad (2.1)$$

where K is a constant multiplicative factor used for changing the scale and x, y are the coordinates of a pixel in image I . The scale space $L(x, y, \sigma)$ of image I is obtained by

$$L(x, y, \sigma) = G(x, y, \sigma) * I(x, y) \quad (2.2)$$

$$G(x, y, \sigma) = \frac{1}{2\pi\sigma^2} e^{-(x^2+y^2)/2\sigma^2} \quad (2.3)$$

where $G(x, y, \sigma)$ is the Gaussian filter for smoothing the image, σ is defined as the width of the filter. This scale invariant technique is found to be suitable for annular iris images because the size of iris changes due to expansion and contraction of the pupil. Figure 2.1 shows the Gaussian blurred iris images and computation of DoG. These images are generated using SIFT code [42].

Keypoint Localisation

DoG images are used to detect interest points with the help of local maxima and minima across different scales. Each pixel in DoG image is compared to 8 neighbors in the same scale and 9 neighbors in the neighboring scales. The pixel is selected as a candidate keypoint if it is local maxima or minima in $3 \times 3 \times 3$ region, as shown in Figure 2.2. Once the keypoints are detected the next step is to perform the detailed fit to the nearby data for the location. The basic idea is to reject keypoints with low contrast. Keypoints with low contrast, are sensitive to noise and poorly localized, hence should not be considered [4].

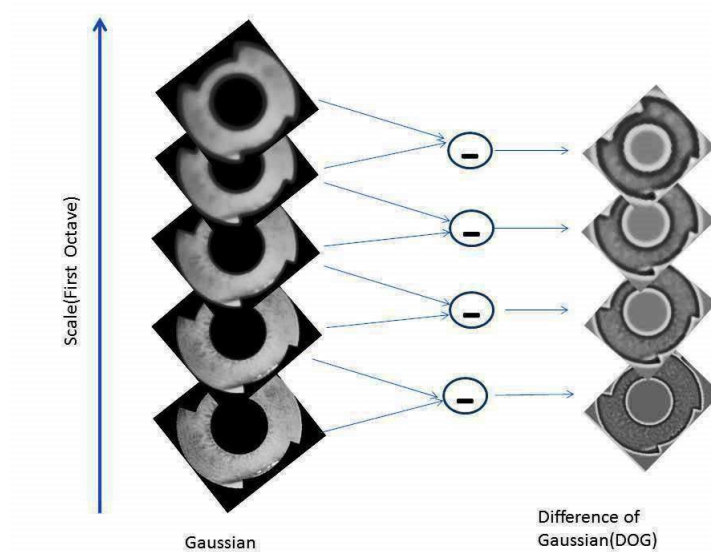


Figure 2.1: Gaussian blurred iris images (left), and Gaussian images are subtracted to produce DoG images (right).

Orientation Assignment

Orientation is assigned to each keypoint location to achieve invariance to image rotations, as descriptor can be represented relative to the orientation. To determine keypoint orientation, a gradient orientation histogram is computed in the neighborhood of keypoint. The scale of keypoint is used to select Gaussian smoothed image L . For each Gaussian smoothed image $L(x, y)$, magnitude $m(x, y)$ and orientation $\theta(x, y)$ are computed as

$$m(x, y) = \sqrt{(L(x+1, y) - L(x-1, y))^2 + (L(x, y+1) - L(x, y-1))^2} \quad (2.4)$$

$$\theta(x, y) = \tan^{-1} \left(\frac{(L(x, y+1) - L(x, y-1))}{(L(x+1, y) - L(x-1, y))} \right) \quad (2.5)$$

Orientation histogram is then formed for gradient orientation around each keypoint. The histogram has 36 bins for 360 orientations. Each sample is weighted by gradient magnitude and a Gaussian weighted circular window with σ on the scale of keypoint, before adding it to histogram. Peaks in the histogram correspond to the orientation and any other local peak within 80% of largest peak is used to create keypoint with the computed orientation. This is done to increase the stability during matching [4]. The scale and direction of orientation is shown in Figure 2.3.

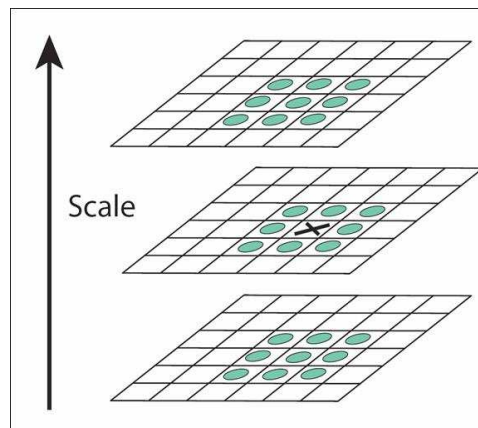


Figure 2.2: Maxima and minima of DoG images are obtained by comparing a pixel to 26 neighbors in $3 \times 3 \times 3$ regions [4]

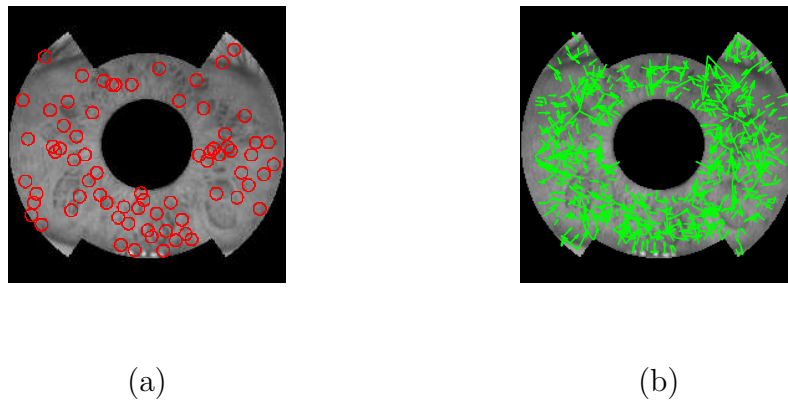


Figure 2.3: Keypoint detection on an annular iris image using SIFT (a) Detected keypoints after removing noise and edge responses, (b) Scale and direction of orientation (indicated by arrows).

2.1.2 Keypoint Descriptor

The feature descriptor is computed as a set of orientation histograms on 4×4 pixel neighborhoods. The orientation histograms are relative to the keypoint orientation as shown in Figure 2.4. The histogram contains 8 bins and each descriptor contains an array of 16 histograms around the keypoint. This generates SIFT feature descriptor of $4 \times 4 \times 8 = 128$ elements. The descriptor vector is invariant to rotation, scaling, and illumination.

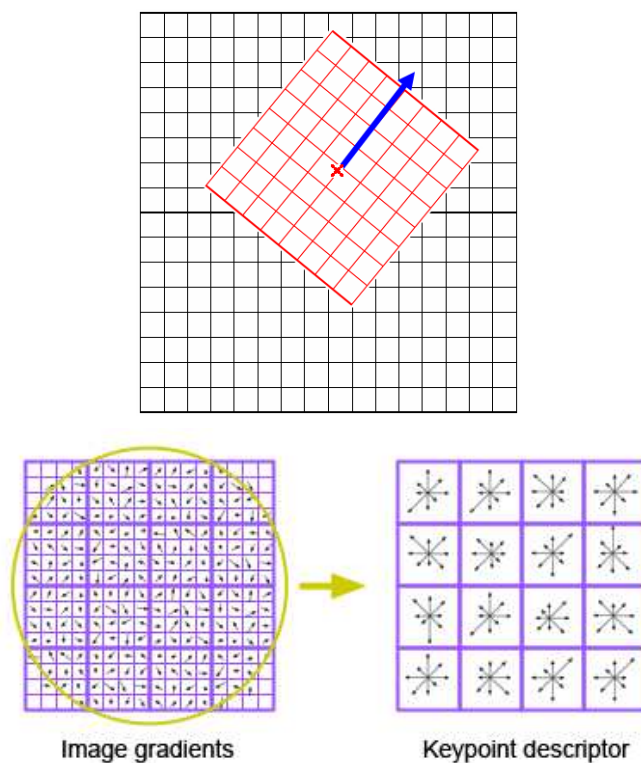


Figure 2.4: Window is taken relative to direction of dominant orientation. This window is weighted by a Gaussian and histogram is obtained for 4×4 regions [2].

2.1.3 Keypoint Pairing

Let $p = \{p_1, p_2, p_3 \dots p_n\}$ and $q = \{q_1, q_2, q_3 \dots q_n\}$ be a n dimensional feature descriptor for each point from the database as well as query images respectively. The Euclidean distance $d(p, q)$ between p and q is defined as

$$d(p, q) = \sqrt{\sum_{i=1}^n (p_i - q_i)^2} \quad (2.6)$$

where n is the dimension of feature descriptor. The naive approach to nearest neighbor matching is to simply iterate through all points in the database to determine the nearest neighbor.

2.2 Speeded Up Robust Features (SURF)

SURF features are not only faster, but far more repeatable and distinctive [5], compared to existing keypoint detectors [4, 43, 44]. SURF use Hessian based detectors,

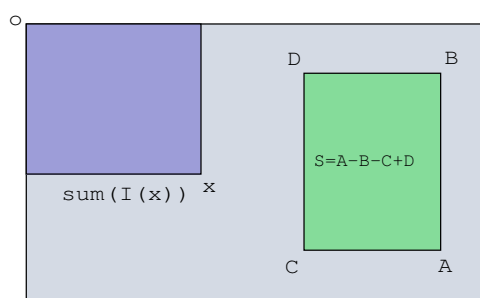


Figure 2.5: Integral images are used to calculate the sum of intensities inside a rectangular region of any size [2].

these are more stable and repeatable than their Harris-based counterparts. SURF uses only 64 dimensions compared to 128 dimensional descriptor vector in SIFT. SURF extracts keypoints using Hessian matrix and describes a distribution of Haar wavelet responses from a window around the interest point as descriptors. Local descriptor vector is computed in two steps: (1) Detection of keypoints (2) Keypoint descriptor. The above mentioned steps are explained as follows.

2.2.1 Detection of Keypoints

Integral images [45] are used for faster computation of interest points. Integral images reduce the computation time drastically by allowing the faster computation of box type convolution filters [6, 46].

Integral Images

The entry of an integral image $I_{\Sigma}(x)$ at a location $x = (x, y)$, represents the sum of all pixels in the input image I within a rectangular region formed by the origin and x

$$I_{\Sigma}(x) = \sum_{i=0}^{i \leq x} \sum_{j=0}^{j \leq y} I(x, y) \quad (2.7)$$

Once the integral image has been computed, the sum of intensities over the integral area can be computed in three additions as shown in Figure 2.5. Thus, the calculation time is independent of the size of the filter.

Interest Points Detection

Hessian matrix based detection is used because of its enhanced performance. For detection of keypoints determinant of the Hessian matrix is computed for selecting location and scale. Given a point $P(x, y)$ in an image I , the Hessian matrix $H(P, \sigma)$ in P at scale σ is defined as,

$$H(P, \sigma) = \begin{bmatrix} L_{xx}(P, \sigma) & L_{xy}(P, \sigma) \\ L_{xy}(P, \sigma) & L_{yy}(P, \sigma) \end{bmatrix} \quad (2.8)$$

where $L_{xx}(P, \sigma)$ is the convolution of the Gaussian second order derivative ($\frac{\sigma^2}{\sigma x^2}g(\sigma)$) with the image I at the point P and similarly $L_{xy}(P, \sigma)$ and $L_{yy}(P, \sigma)$ are obtained. The Gaussian is discretised and cropped as shown in Figure 2.6. These approximate Gaussian second order derivatives can be evaluated at a very low computational cost using integral images. The 9×9 box filters as shown in Figure 2.6 are approximations of a Gaussian at $\sigma = 1.2$. These are denoted by D_{xx} , D_{xy} , and D_{yy} [47]. By choosing the weights for the box filters adequately, the approximations for the Hessian's determinant are computed using

$$Det(H_{approx}) = D_{xx}D_{yy} - (0.9D_{xy})^2 \quad (2.9)$$

Scale Space Representation

Due to the use of integral image and box filters, it is not required to iteratively apply the same filter to the output of the previously filtered image. This can be made computationally efficient by applying box filter of any size on the original image as shown in Figure 2.7. Therefore scale space is analyzed by upscaling the filter size

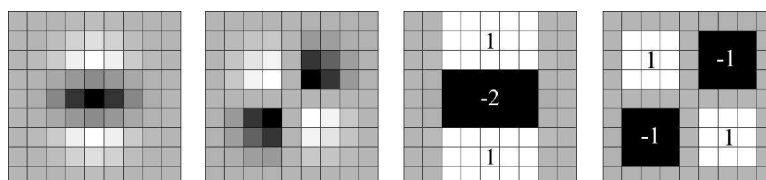


Figure 2.6: Left to right: discrete Gaussian second order derivative in y and xy direction. Approximation for the second order Gaussian partial derivative in y -direction (D_{yy}) and xy -direction (D_{xy}) [5].

rather than reducing the image size. The output of the 9×9 filter, introduced in the previous section, is considered as the initial scale layer. Subsequent layers are obtained by filtering the image with larger masks to localize keypoints invariant to scale. The advantage of such scale space creation is that it is computationally efficient as the image is not down-sampled so there is no effect of aliasing.

The scale space is divided into *octaves*. Each octave is represented by a series of responses obtained by convolving the input image with filter of increasing size. Each octave is subdivided into a constant number of scale levels. The length (l_0) of a positive or negative lobe of partial second order derivative in the direction of derivation (x or y) is set for third of the filter size length. For the 9×9 filter, this length l_0 is 3. For two successive levels, the size is increased by a minimum of two pixels in order to keep the filter size an odd value and thus ensure the presence of the central pixel. This results in a total increase of the mask size by six pixels as shown in Figure 2.8.

Scale space construction starts with the initial 9×9 filter for which scale $s=1.2$. Then, filters with sizes 15×15 , 21×21 , and 27×27 are applied, by which even more than a scale change of two has been achieved. The filter size increase is doubled for every new octave (from 6-12 to 24-48). The filter size is increased for corresponding octaves until image size is larger than the filter size.

Keypoint Localisation

Interest points are localized in scale and image space by applying a non maximum suppression in a $3 \times 3 \times 3$ neighborhood. The local maxima found on the Hessian matrix determinant are interpolated to image space as proposed in [48]. Figure 2.9 shows the

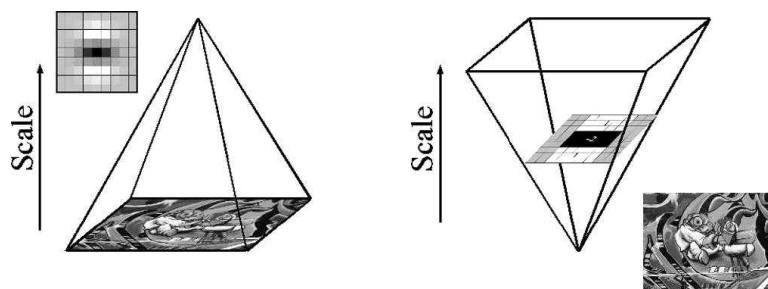


Figure 2.7: Use of integral images for upscaling filter masks [6].

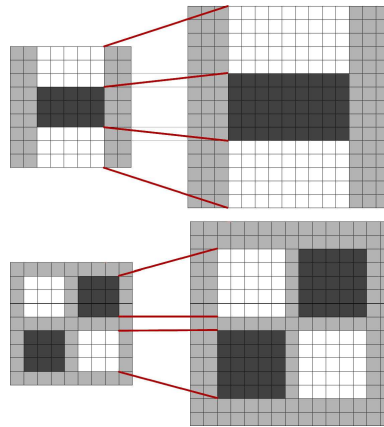


Figure 2.8: Filters D_{yy} (top) and D_{xy} (bottom) for two successive filter sizes (9×9 and 15×15) [6].

detected interest points on the annular iris image.

2.2.2 Keypoint Descriptor

Descriptor of every interest point is computed using Haar wavelet responses in x and y directions. The descriptor size kept only 64 dimensions for fast operation. The first step consists of finding orientation using a circular window around the keypoint. Then, a square region aligned with the selected orientation is considered to extract the keypoint descriptor.

Orientation Assignment

To achieve invariance to image rotation, the orientation is identified for each keypoint. For this purpose, Haar wavelet responses are calculated in x and y direction within a

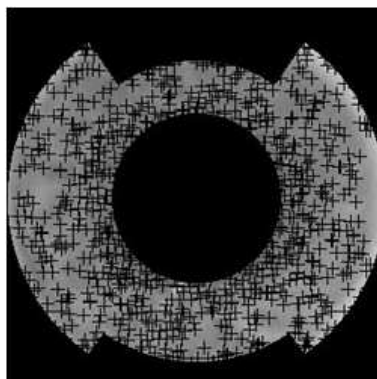


Figure 2.9: SURF detected keypoints on the annular iris image.

circular neighborhood of radius $6s$ around the keypoint, with s as the scale at which the interest point was detected. The size of wavelets is scale dependent and set to side length of $4s$. Once the wavelet responses are calculated and weighted with a Gaussian ($\sigma = 2s$), the common orientation is obtained by calculating the sum of all responses within a sliding orientation window of size $\frac{\pi}{3}$ as shown in Figure 2.10. The horizontal and vertical responses within the window are summed. The longest such vector over all windows defines the orientation.

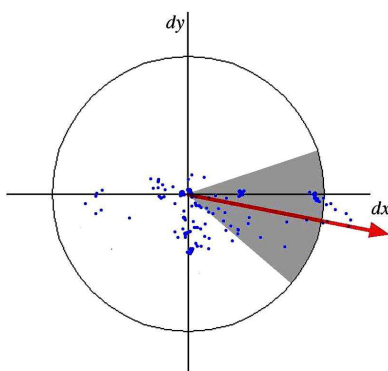


Figure 2.10: Orientation assignment by taking a sliding window of size $\frac{\pi}{3}$ indicated by shaded region [6].

Keypoint Descriptor

The descriptor vector is obtained around every detected interest point by taking a square window of size $20s$ centered around the keypoint and aligned relative to the direction of orientation. As shown in Figure 2.11 the region is split into 4×4 smaller sub-regions to preserve the spatial information. For each sub-region, Haar wavelet responses are obtained in horizontal (d_x) and vertical direction (d_y). To increase the robustness towards localization errors and geometric deformations, the responses d_x and d_y are first weighted with a Gaussian ($\sigma = 3.3s$) centered at the keypoint.

Finally, the feature vector is summed up for each sub-region to form the elements of descriptor vector D_v . The sum of the absolute values of the responses are obtained ($|d_x|$ and $|d_y|$), to know the information about the polarity of the intensity changes. Thus, each sub-region is a 4D descriptor vector D_v comprising of

$$D_v = \left\{ \sum d_x, \sum d_y, \sum |d_x|, \sum |d_y| \right\} \quad (2.10)$$

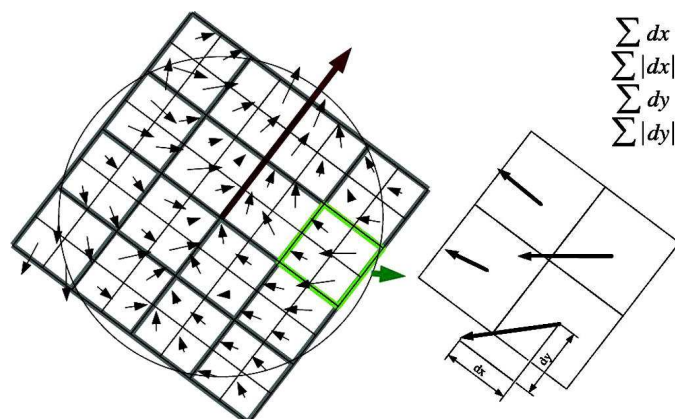


Figure 2.11: An oriented window with 4×4 sub-regions is taken in the direction of orientation. For each sub-region wavelet responses are obtained [6].

Concatenating this for all 4×4 sub-regions results in a feature vector of length 64.

2.2.3 Keypoint Pairing

After detection of interest points in database image (A) and query image (B), matching is carried out using interest point pairing approach. The best candidate match for each keypoint in A is found by identifying the closest pair from the set of keypoints in B . The nearest neighbor is defined as the keypoint with minimum Euclidean distance for the invariant descriptor vector. Let $L = \{l_1, l_2, l_3, \dots, l_m\}$ and $E = \{e_1, e_2, e_3, \dots, e_n\}$ be vector arrays of keypoints of A and B respectively obtained through SURF.

The descriptor arrays l_i of keypoint i in L and e_j of keypoint j in E are paired if the Euclidean distance $\|l_i - e_j\|$ between them is less than a specified threshold τ . Threshold based pairing results in several numbers of matching points. To avoid multiple matches, the keypoints with minimum descriptor distance compared with threshold and if it is less than the threshold then they are paired. This results in a single pair, and is called as nearest neighborhood matching method. The matching method applied in SURF is similar to the nearest neighbor matching, except that the thresholding is applied to the descriptor distance ratio between keypoints. The method used in SURF is called as a nearest neighbor ratio method. Thus, the interest points are matched as,

$$\frac{\|l_i - e_j\|}{\|l_i - e_k\|} < \tau \quad (2.11)$$

where, e_j is the first nearest neighbor and e_k is the second nearest neighbor of l_i . The paired points (l_i, e_j) are removed from L and E respectively. The matching process is continued until there are no more interest points. Based on the number of pairs between query image A and database image B , a decision is taken about a candidate's identity.

2.3 Binary Robust Invariant Scalable Keypoints (BRISK)

The inherent difficulty in extracting suitable features from an image lies in balancing two competing goals: high quality description and low computational requirements. SURF has been demonstrated to achieve robustness and speed, but BRISK achieves comparable quality of matching at a much less computation time. There are two steps involved to determine local descriptor vector and they are (1) Scale-space keypoint detection and (2) Keypoint description. The details of the steps are explained as follows.

2.3.1 Keypoint Detection

With the focus on computation efficiency, BRISK detection methodology is inspired by the work of Mair *et al.* [49], for detecting regions of interest in the image. Their *Adaptive and generic corner detection based on the accelerated segment test* (AGAST) is essentially an extension for accelerated performance of the now popular FAST [41]. With the purpose of achieving invariance to scale, which is important for high-quality interest points, the BRISK go a step further by searching for maxima not only in the image plane, but also in scale-space using the FAST scores s as a measure for saliency. The BRISK detector estimates the true scale of each keypoint in the continuous scale-space. In the BRISK framework, the scale-space pyramid layers consist of n octaves c_i and n intra-octaves d_i , for $i = \{0, 1, \dots, n - 1\}$ and for typically $n = 4$. The octaves are formed by progressively half-sampling the original image (corresponding to c_0). Each intra-octave d_i is located in-between layers c_i and c_{i+1} as shown in Figure 2.12. The first intra-octave d_0 is obtained by down-sampling the original image c_0 by a

factor of 1.5, while the rest of the intra-octave layers are derived from successive half-sampling [7]. The t denotes scale, then $t(c_i) = 2^i$ and $t(d_i) = (1.5) \times 2^i$.

The BRISK use 9-16 mask, which essentially requires at least 9 consecutive pixels in the 16-pixel circle to either be sufficiently brighter or darker than the central pixel, for the FAST criterion to be fulfilled. Initially, the FAST 9-16 detector is applied on each octave and intra-octave separately using the same threshold to identify the potential regions of interest. Next, the points belonging to these regions are subjected to a non-maxima suppression in scale-space. Firstly, the maximum condition needs to fulfill with respect to its 8 neighboring FAST scores s in the same layer [7]. Secondly, the scores in the layer above and below will need to be lower as shown in Figure 2.12.

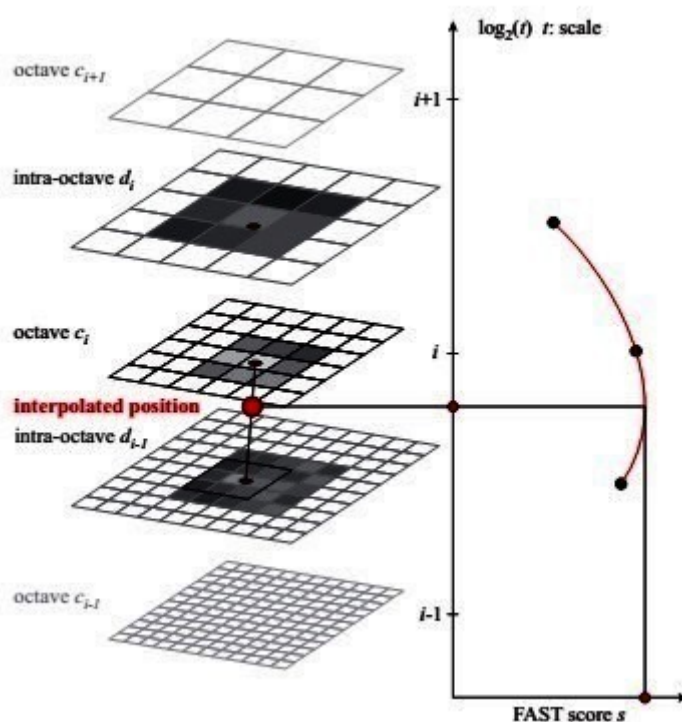


Figure 2.12: Scale-space interest point detection: a keypoint is identified at octave c_i by analyzing the 8 neighboring saliency scores in c_i as well as in the corresponding scores-patches in the immediately-neighboring layers above and below [7].

2.3.2 Keypoint Description

The BRISK descriptor vector is a binary string, obtained by concatenating the results of simple brightness comparison tests. In BRISK, the characteristic direction

of each keypoint is computed to achieve rotation invariance, which is key to general robustness. Also, the brightness comparisons are carefully selected with the focus on maximizing descriptiveness.

Sampling Pattern and Rotation Estimation

The key concept of the BRISK descriptor makes use of a pattern used for sampling the neighborhood of the interest point. The pattern, defines N_l locations equally spaced on circles concentric with the keypoint as shown in Figure 2.13. In order to prevent aliasing effects when sampling the image intensity of a point p_i in the pattern, Gaussian smoothing is applied with standard deviation σ_i proportional to the distance between the points on the respective circle.

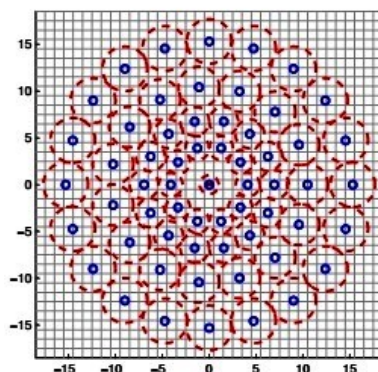


Figure 2.13: The BRISK sampling pattern with $N_l = 60$ points: the small blue circles denote the sampling locations; the bigger, red dashed circles are drawn at a radius σ corresponding to the standard deviation of the Gaussian kernel used to smooth the intensity values at the sampling points [7].

Positioning and scaling the pattern accordingly for a particular interest point k in the image. The N number of circles are drawn at a radius σ corresponding to the standard deviation of the Gaussian kernel, used to smooth the intensity values at the sampling points. By taking one of the $N_l \cdot (N_l - 1) / 2$ sampling-point pairs (p_i, p_j) into consideration. The smoothed intensity values at these points which are $I(p_i, \sigma_i)$ and $I(p_j, \sigma_j)$ respectively, are used to estimate the local gradient $g(p_i, p_j)$ by

$$g(p_i, p_j) = (p_j - p_i) \cdot \frac{I(p_j, \sigma_j) - I(p_i, \sigma_i)}{\|p_j - p_i\|^2} \quad (2.12)$$

Considering the set A of all sampling-point pairs:

$$A = \{(p_i, p_j) \in \mathbb{R}^2 \times \mathbb{R}^2 \mid i < N_l \wedge j < i \wedge i, j \in \mathbb{N}\} \quad (2.13)$$

The subset of short-distance pairings is S and another subset of L number of long-distance pairings is \mathcal{L} :

$$S = \{(p_i, p_j) \in A \mid \|p_j - p_i\| < \delta\} \subseteq A \quad (2.14)$$

$$\mathcal{L} = \{(p_i, p_j) \in A \mid \|p_j - p_i\| > \delta\} \subseteq A \quad (2.15)$$

The threshold distance are set to $\delta = 9.75t$ (t is the scale of k). Iterating through the point pairs in \mathcal{L} , the overall characteristic pattern direction of the keypoint k computed as,

$$g = \begin{pmatrix} g_x \\ g_y \end{pmatrix} = \frac{1}{L} \cdot \sum_{(p_i, p_j) \in \mathcal{L}} g(p_i, p_j) \quad (2.16)$$

Building the Descriptor

For the formation of the rotation and scale-normalized descriptor, BRISK applies the sampling pattern rotated by $\alpha = \arctan2(g_y, g_x)$ around the interest point k . The descriptor vector d_k is assembled by performing all the short-distance intensity comparisons of point pairs $(p_i^\alpha, p_j^\alpha) \in S$, such that each bit b corresponds to:

$$b = \begin{cases} 1, & I(p_j^\alpha, \sigma_j) > I(p_i^\alpha, \sigma_i) \\ 0, & \text{otherwise} \end{cases} \quad \forall (p_i^\alpha, p_j^\alpha) \in S \quad (2.17)$$

2.3.3 Descriptor Matching

Matching two BRISK descriptor bit-vectors is a simple calculation of their Hamming distance. The number of bits different in the two descriptor vectors is a measure of their dissimilarity. The respective operations reduce to a bitwise *XOR* followed by a bit count, which can both be computed very efficiently. BRISK interest point matching on two annular iris images is shown in Figure 2.14.

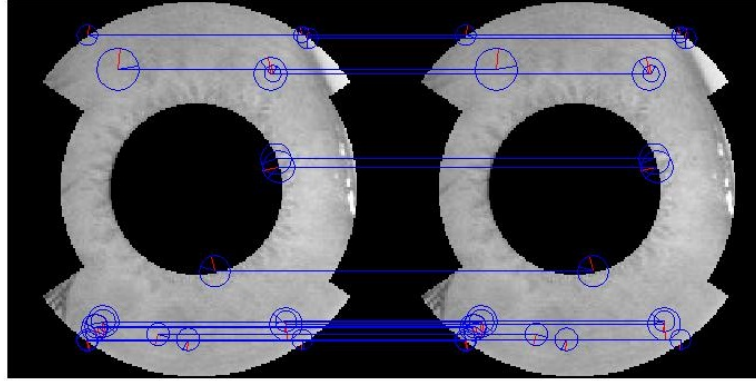


Figure 2.14: BRISK interest point matching on two annular iris images.

A comparative study of SIFT, SURF, and BRISK based on feature extraction and matching techniques is shown in Table 2.1. DoG, Hessian matrix, and FAST techniques are used for keypoint detection in SIFT, SURF, and BRISK respectively. Oriented histogram, Haar wavelet, and intensity comparisons are used for feature vector generation in SIFT, SURF, and BRISK respectively. SIFT and SURF use Euclidean distance, and BRISK use hamming distance for descriptor vector matching. In Table 2.2, comparison of SIFT, SURF, and BRISK feature extraction techniques is shown using a single CASIA iris image. By studying this table, it is well understood that SIFT is a very slow process because it detects a high number of keypoints and its descriptor dimension is 128. SURF is faster than SIFT but take more computation time than BRISK. Both SURF and BRISK have 64 dimensional descriptors. BRISK is faster than SIFT and SURF because its descriptor is a 64 bit string.

Table 2.1: Comparative study of SIFT, SURF, and BRISK based on feature extraction and matching techniques.

	Keypoint Extraction Technique	Feature Vector Generation	Matching Technique
SIFT	DoG	Oriented Histogram	Euclidean Distance
SURF	Hessian matrix	Haar wavelet	Euclidean Distance
BRISK	FAST	Intensity Comparisons	Hamming Distance

Table 2.2: Comparative of SIFT, SURF, and BRISK for a single CASIA iris image.

Feature Extraction Technique	Detected Keypoints	Dimension of Descriptor	Elapsed Time (in seconds)
SIFT	403	128	31.953
SURF	56	64	1.150
BRISK	20	64	0.125

2.4 Summary

In this chapter, three well known keypoint descriptors are studied and applied to iris. In order to achieve scale invariance, SIFT is applied to annular iris that is robust to all possible transformations as well as partial occlusion. The time required to recognize an individual is more due to higher dimensionality of feature descriptor. SURF performs better compared to existing keypoint descriptors in terms of reliability, accuracy, and speed. Further, the time required to claim identification using SURF is reduced because it detects less number of keypoints and lower dimensionality of feature descriptor than SIFT. One of the recently developed keypoint descriptor coined BRISK is also applied to annular iris. Based on the experimental study it has been inferred that BRISK is faster than previously existing techniques because it uses a bit string as a feature descriptor.

Chapter 3

Iris Identification

During identification, an individual candidate is recognized by searching the templates of all the users in the database for a match. Therefore, the system conducts a one to many comparisons to find an individual's identity. The identification system suffers from an overhead of large number of comparisons in the database. As the size of database increases the time required to declare an individual's identity increases significantly [50]. Thus, accuracy can be improved by reducing search space. The retrieval time can be reduced by using classification, clustering and indexing approaches on the database. Biometrics does not possess any natural or alphabetical order. Iris biometric system uses collection of image templates as database. Traditional database indexing schemes do not work in content based image retrieval (CBIR) system. Thus, the query feature vector is compared sequentially with the all templates in the database. The retrieval efficiency in sequential search depends upon the database size. This leaves behind a challenge to develop a non-traditional indexing scheme that reduces the search space in the large biometric database. The general idea of indexing is to store closely related feature vectors together in the database at the time of enrollment. During identification, the part of the database that has close correspondence with query feature vector is searched to find a probable match. In the proposed work, two indexing schemes known as Geometric Hashing [30, 51] and Enhanced Geometric Hashing [33] are applied on locally detected keypoints, to render an efficient iris identification system. The two identification approaches and their comparison based on simulation results are discussed in sequel.

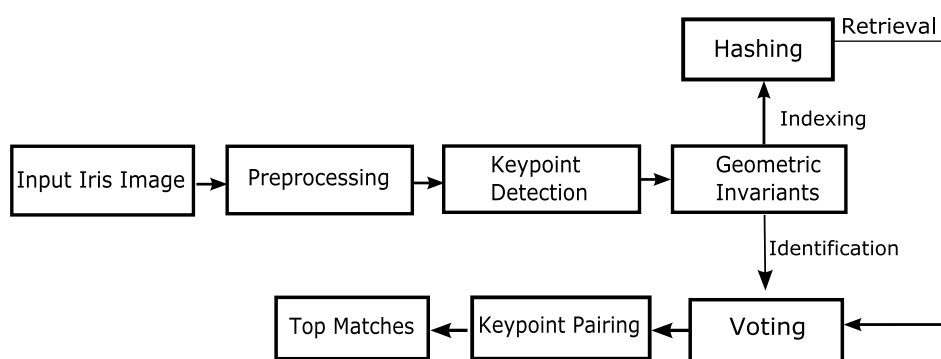


Figure 3.1: Block diagram for geometric hashing based indexing approach [3].

3.1 Indexing based on Geometric Hashing

Geometric hashing is an indexing technique for model based object recognition that uses location of keypoints which are invariant to similarity transformation [30, 51]. During image retrieval, keypoint locations are computed for the query image and are used to index into the hash table to find the possible matches [52]. The primary advantage of geometric hashing is that it speeds up the search and recognizes the object efficiently. The block diagram of geometric hashing based indexing approach is given in Figure 3.1. The keypoints are detected directly from noise independent annular iris image using local feature extraction. Geometric invariants are obtained for detected keypoints and stored in the quantized hash table during indexing. During identification, the hash table is accessed using the invariants and votes are casted. Entries that receive more than certain number of votes are considered as candidate irises. The steps involved in indexing are explained in the following subsections.

3.1.1 Indexing

The geometric hashing scheme allows for retrieval of model images that differ from query image by some kind of similarity transformation like rotation and scaling [53]. It is used for model based object recognition that forms indices from a subset of model points. One of the advantages of geometric hashing is that it is inherently parallel. It has been observed in [54] that with minimal communication and maintenance costs, the concept of geometric hashing is parallel and can be shared among number of cooperating processors. Further, the technique remains invariant to similarity

transformations and its representation performs well under partial occlusion.

Index Generation

The detected interest points on annular iris image are used for indexing the database. The basic idea is to extract local features from an image that remain invariant to similarity transformations. The property of invariance can be explained with the help of a model. The points detected from a sample iris image are plotted on a two dimensional plane and represent a model (M_i) of i^{th} image in the database as shown in Figure 3.2(a). A pair of keypoints (k_1 and k_2) is chosen as an ordered basis as represented in Figure 3.2(a). The keypoints are chosen for different combinations of basis pair with an assumption that k_2 should lie in positive x axis. Thus, for n keypoints the possible basis pairs are at most $\binom{n}{k}$. The keypoints are scaled such that the magnitude of $\overrightarrow{k_1 k_2}$ is equal to 1. The midpoint between k_1 and k_2 is placed at the origin such that k_1 and k_2 have positive x axis. The remaining points of M_i are placed at different locations. For each choice of basis, the remaining points P of model M_i are computed using

$$P = uP_x^i + vP_y^i + P_0^i \quad (3.1)$$

where $P(x, y)$ is the keypoint to be indexed, (u, v) is the location of P after similarity transformation. P_x^i and P_y^i are defined by

$$P_x^i = \frac{k_2 - k_1}{2} \quad (3.2)$$

$$P_y^i = \text{Rot}_{90}(P_x^i) \quad (3.3)$$

where Rot_{90} refers to rotation of coordinate locations by 90 degrees. The midpoint P_0^i between k_1 and k_2 is defined by

$$P_0^i = \frac{k_1 + k_2}{2} \quad (3.4)$$

The keypoints after transformation of model M_i for basis pair k_1 and k_2 are shown in Figure 3.2(b). However, since iris is occluded by upper and lower eyelids thus there is a possibility that the basis (k_1, k_2) may not occur in every instance of model M_i . Therefore, different combinations of possible basis pair are used to obtain the geometric invariants as shown in Figure 3.2(c).

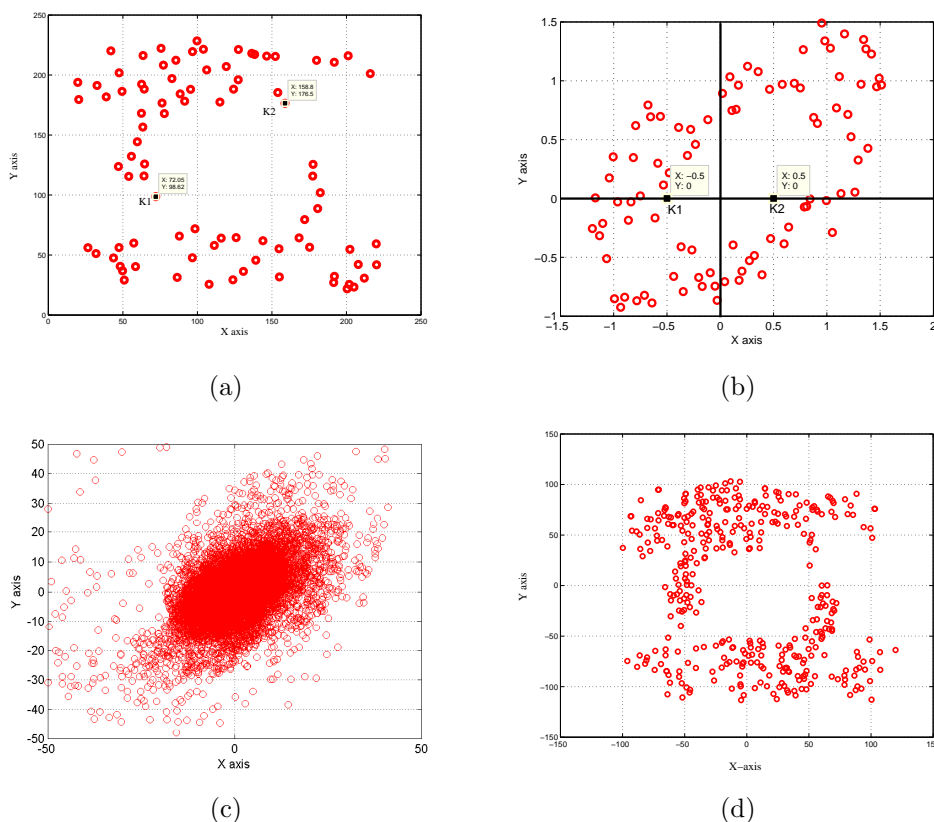


Figure 3.2: Similarity transformation: (a) Two dimensional representation of detected keypoints from annular iris image, (b) Keypoints after similarity transformation for basis pair k_1k_2 , (c) Keypoints after similarity transformation of possible basis pairs, and (d) Keypoints after rehashing.

Hash Table Organization

For the formation of hash table, the possible ordered basis pairs for all model images are selected to obtain transformation invariant coordinates (u, v) of the remaining points (x, y) . The values of u and v computed from equation (3.1) remain invariant under similarity transformation and their quantisation allows to have an index (u_q, v_q) into the hash table. The hash table at (u_q, v_q) contains the entry in the form of (M_i, k_1, k_2) for model M_i with basis pair $\overrightarrow{k_1k_2}$. The hash bin occupancy for quantized hash table is non-uniform. A uniform distribution of entries over hash table is required to reduce the data retrieval and execution time. Thus, Rigoutsos and Hummel [54] have proposed an efficient technique for uniform distribution of entries in the hash table. The distribution of data over quantized hash table follows a Gaussian distribution and keypoints detected from iris undergo similarity transformations. The

probability density $f(u, v)$ can be defined by

$$f(u, v) = \frac{3}{\pi} \frac{1}{(u^2 + v^2 + 3)^2} \quad (3.5)$$

where u and v are invariant coordinates after geometric transformation. After computing the probability density a transformation is performed to map the distribution of entries uniformly in a hash table using rehashing. The rehashing function is applied to transformed coordinates so that equally spaced bins have uniform occupancy as shown in Figure 3.2(d). Rehashing function for similarity transformation is given as [54],

$$h(u', v') = \left(1 - \frac{3}{u^2 + v^2 + 3}, \text{atan2}(v, u)\right) \quad (3.6)$$

where u and v are transformed coordinates and atan2 is four quadrant inverse tangent. This has reduced the accumulation of data at a particular region in the hash table. At $h(u', v')$ an entry is stored in the hash table with (model, basis) pair. The keypoint descriptor obtained using a local feature descriptor is stored in the feature database corresponding to a particular iris image.

3.1.2 Iris Retrieval

During identification, iris images that have close proximity with the query image are retrieved from the database. The query image is preprocessed to detect annular portion of iris. The keypoints are localised on the annular query iris image and arbitrarily two keypoints are chosen as ordered basis pair and transformed such that its midpoint coincides with the center of origin with direction in the positive x axis. The magnitude of basis vector has unit length. The coordinates of remaining keypoints are defined using equation (3.1) for chosen basis pair. Each transformed entry is quantized and mapped to the hash table. For each entry found in the corresponding hash table bin, a vote is casted.

The basic assumption is that in case the query image contains basis that corresponds to that of model image from database, then it is expected to receive votes from all other unoccluded points. The total number of votes for various basis pairs corresponding to each model image is determined. If the number of votes received for each model image are greater than a threshold (τ), then these images are considered

to be potential matches for query image. Further the keypoint descriptor for query and candidate model images are compared to find top best matches.

3.2 Indexing based on Enhanced Geometric Hashing

Most of the indexing techniques work on a fixed number of feature points. However, in biometrics the feature points may vary from image to image, and the maximum number of feature points cannot be predicted in advance. Traditional geometric hashing can be used to index the variable feature points in a high-dimensional space. Traditional geometric hashing may not be suitable for its computational time and memory requirement. Unlike the available geometric hashing, the enhanced geometric hashing requires less amount of time and memory.

3.2.1 Preprocessing

During indexing, the features $\{f_1, f_2, \dots, f_m\}$ are extracted for all annular iris images using local feature extraction techniques [4, 5, 7]. There is a possibility that the model images may appear translated and rotated relative to their original positions. In addition, models may not have the same scale. Hence in order to make the indexing technique invariant to translation, rotation and scaling, every model for the database is preprocessed. It consists of three steps: mean centering, rotation with respect to principal components, and normalization [33].

Mean Centering

whenever the iris image is translated, the feature points are also translated from their original positions. In that case, mean centering can be used to translate each feature point f_i to f'_i such that mean of all f'_i becomes zero. This can be done by subtracting $\bar{f} = \frac{1}{m} \sum_{i=1}^m f_i$ from f_i . A two dimensional representation of BRISK detected keypoints from an annular iris image are shown in Figure 3.3(a). In Figure 3.3(b) keypoints are plotted after mean centering.

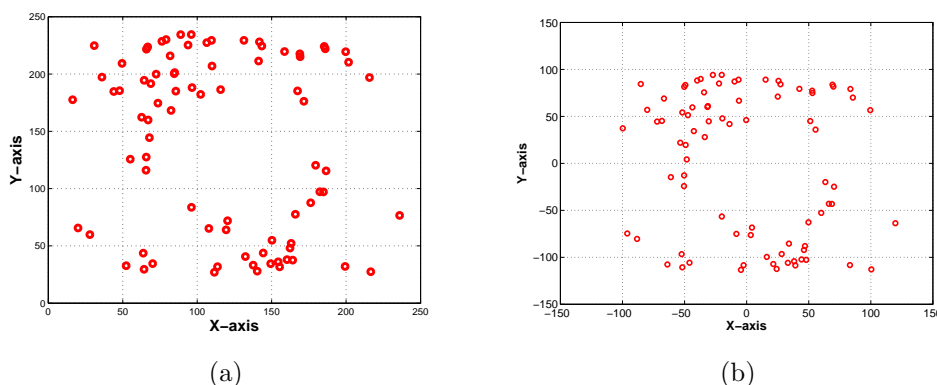


Figure 3.3: (a) Two dimensional representation of detected keypoints from annular iris image, (b) Keypoints after mean centering.

Rotation with respect to Principal Components

The set of feature points $\{f'_1, f'_2, \dots, f'_m\}$ is used to determine the largest PC_1 and the second largest PC_2 principal components [33]. Principal components are computed by using the matrix $A = \begin{bmatrix} f'_1 & f'_2 & \dots & f'_m \end{bmatrix}$. First, covariance matrix $C = \frac{1}{m} \sum_{j=1}^m f'_j f'_j{}^T = AA^T$ is calculated, then eigenvalues of C are calculated and arranged in decreasing order ($\lambda_1 > \lambda_2 > \dots > \lambda_n$). Second, eigenvectors (u_1, u_2, \dots, u_n) obtained using corresponding eigenvalues. These eigenvectors are principal components of matrix A. This transformation is defined in such a way that the first principal component has the largest possible variance, and each succeeding component in turn has the highest variance possible under the constraint, that it be orthogonal to the preceding components. The geometric properties of PCA are used to make the iris images invariant to rotation. PC_1 and PC_2 , are rotated in such a way that they become the primary axes of the co-ordinate system. After rotation step, point set $\{f'_1, f'_2, \dots, f'_m\}$ become $\{f''_1, f''_2, \dots, f''_m\}$ as shown in Figure 3.4(a).

Normalization

In order to make the feature points invariant to scale, the normalization step is carried out. For the point set $\{f''_1, f''_2, \dots, f''_m\}$ each feature point is divided by the standard deviation (σ) of the point set and multiplied by some scaling factor α , such that every feature point gets different bin into the hash table. The point set $\{f''_1, f''_2, \dots, f''_m\}$ becomes $\{f'''_1, f'''_2, \dots, f'''_m\}$ after normalization as shown in Figure 3.4(b).

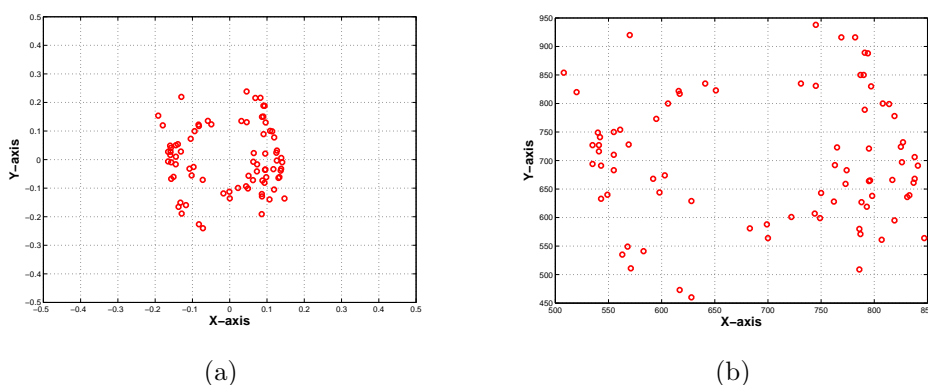


Figure 3.4: (a) Keypoints after rotation with respect to principal components, (b) Keypoints after normalization.

3.2.2 Hash Table Generation

Now each feature point is mapped into the location p_l of hash table by placing the midpoint of the co-ordinate system at the center of the hash table as follows:

$$p_l = f_l''' + \frac{size(H)}{2} \quad (3.7)$$

where $size(H)$ is the number of bins in the hash table H . After mapping, all feature points are inserted into hash table as

$$H(p_l) = H(p_l) \cup (M_{id}, \vec{D}) \quad (3.8)$$

where M_{id} and \vec{D} are the model identity and the descriptor vector of the feature point respectively. The same process is repeated for each model in the database.

3.2.3 Searching

For a query Q , the top t_k best matches from the hash table are obtained in two steps such as filtering and refinement. In the filtering step, the feature points which are dissimilar to the query feature points are filtered out while at refinement step, the top t_k matches are found based on the voting scheme.

Filtering

In this step, the feature points of the model which are dissimilar to the query feature points are filtered out based on their descriptor vector \vec{D} . It is observed that the

feature points of the different images of the same model may be missed due to the noise present in the images. With the objective of improved recognition performance, it considers the feature points not only from its mapped bin but also from its nearest bins of window size $w \times w$. Suppose $\{f_1, f_2, \dots, f_n\}$ be the n feature points in the query. For a feature point f_i , let q be the mapped index in the hash table H . Let z be a neighboring bin, $z \in [q - \frac{w}{2}, q + \frac{w}{2}]$. There may be some feature points of different models from the database lying in the bin z of H . Let c be a feature point of a model lying in z . Euclidean distance $d(c)$ between q and c , $\forall c \in H(z)$ can be obtained by the following equation,

$$d(c) = \|\vec{D}(q) - \vec{D}(c)\| \quad (3.9)$$

A candidate set C_i for the corresponding feature point f_i of the query Q contains all the model identity $M_{id}(c)$ such that $d(c) \leq \tau$, where τ is the threshold value. The same procedure is followed for all query feature points $\{f_1, f_2, \dots, f_n\}$. Therefore, there are n candidate sets $\{C_1, C_2, \dots, C_n\}$ for given n feature points in a query Q .

Refinement

In this step, the candidate sets $\{C_1, C_2, \dots, C_n\}$ are concatenated and the number of occurrences of each model identity M_{id} is determined. Let C be the set of the form $C = (M_{id}, l)$, where l is the number of occurrence of each model identity M_{id} . The elements of C are arranged in decreasing order with respect to the number of occurrences. First t_k model identities of the set C are considered as top t_k matches against the query Q .

3.3 Comparative analysis of Geometric Hashing and Enhanced Geometric Hashing

In this section, comparative analysis of geometric hashing and enhanced geometric hashing schemes using local features of annular iris is discussed. First, SIFT features of annular iris are considered as local features. Second, experiments performed using SURF features. At last, BRISK keypoints are used as feature points. The time taken in binning of a single image for different databases are shown in Table 3.1.

Table 3.1: The time taken in binning of a single image for different databases.

Iris Database	Geometric Hashing (elapsed time in millisecond)	Enhanced Geometric Hashing (elapsed time in millisecond)
BATH	186	102
CASIA	20606	592
IITK	21809	513
UBIRIS	4365	209

3.3.1 Comparative analysis using SIFT

Geometric hashing with one of the well known keypoint descriptor known as SIFT has been applied to iris for feature extraction and matching. Geometric hashing performs with maximum identification probabilities 0.69, 0.74, 0.48, and 0.80 with respect to UBIRIS, BATH, CASIA, and IITK iris datasets respectively, by taking top 100 ranks into consideration. Enhanced geometric hashing achieves maximum identification probabilities 0.79, 0.91, 0.82, and 0.97 with respect to UBIRIS, BATH, CASIA, and IITK iris datasets respectively, by taking top 100 ranks into consideration as shown in Table 3.2. For each iris database accuracy of enhanced geometric hashing is better than traditional geometric hashing as shown in Figure 3.5. For BATH iris database graph of enhanced geometric hashing is monotonically increasing up to rank 10 and after that it is constant at identification probability 0.95 and geometric hashing graph attain 0.75 identification probability after 100 ranks as shown in Figure 3.5(a). Experimental results for CASIA, IITK, and UBIRIS iris databases are shown in Figure 3.5(b), Figure 3.5(c), and Figure 3.5(d) respectively.

Table 3.2: Identification probabilities at various ranks for geometric hashing (GH) and enhanced geometric hashing (EGH) using SIFT keypoints.

Ranks	UBIRIS		BATH		CASIA		IITK	
	GH	EGH	GH	EGH	GH	EGH	GH	EGH
1	0.3594	0.1083	0.0851	0.1064	0.02878	0.04317	0.2826	0.1739
2	0.4009	0.2083	0.1277	0.383	0.03597	0.1727	0.3261	0.6957
3	0.4239	0.3083	0.1702	0.4255	0.04317	0.2446	0.3478	0.6957
5	0.4700	0.3833	0.3404	0.5745	0.0575	0.3309	0.4348	0.7391
10	0.5299	0.4833	0.4468	0.8936	0.1367	0.4173	0.5217	0.8261
20	0.5668	0.7167	0.5319	0.9149	0.2374	0.5468	0.7174	0.8696
30	0.6037	0.7917	0.617	0.9149	0.2806	0.6403	0.42857	0.8913
50	0.6498	0.7917	0.7234	0.9149	0.3597	0.6978	0.8043	0.9348
100	0.6959	0.7917	0.7447	0.9149	0.482	0.8273	0.8043	0.9783

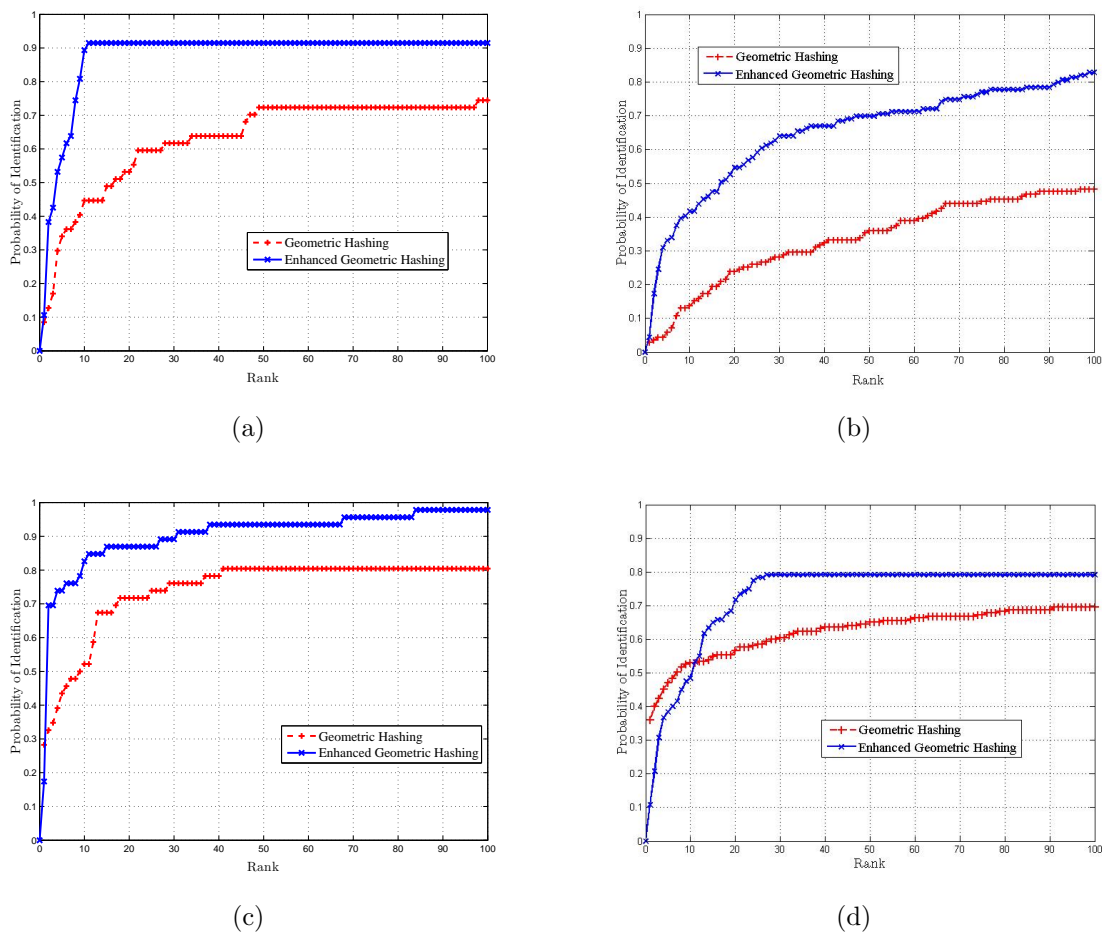


Figure 3.5: CMC curve for geometric hashing and enhanced geometric hashing using SIFT on different iris databases, (a) BATH, (b) CASIA, (c) IITK, and (d) UBIRIS.

3.3.2 Comparative analysis using SURF

In this section, SURF is applied with geometric hashing and enhanced geometric hashing in a comparative manner. Geometric hashing performs with maximum identification probabilities 0.29, 0.55, 0.38, and 0.57 with respect to UBIRIS, BATH, CASIA, and IITK iris datasets respectively. Enhanced geometric hashing achieves maximum identification probabilities 1, 0.79, 0.9, and 0.75 with respect to UBIRIS, BATH, CASIA, and IITK iris datasets respectively, by taking top 100 ranks into consideration as shown in Table 3.3. As shown in Figure 3.6(d), for UBIRIS iris database enhanced geometric hashing attains identification probability 1 quickly but traditional geometric hashing performance is not so good. Figure 3.6(a) for BATH iris database also shows that enhanced geometric hashing is better than traditional geometric hashing.

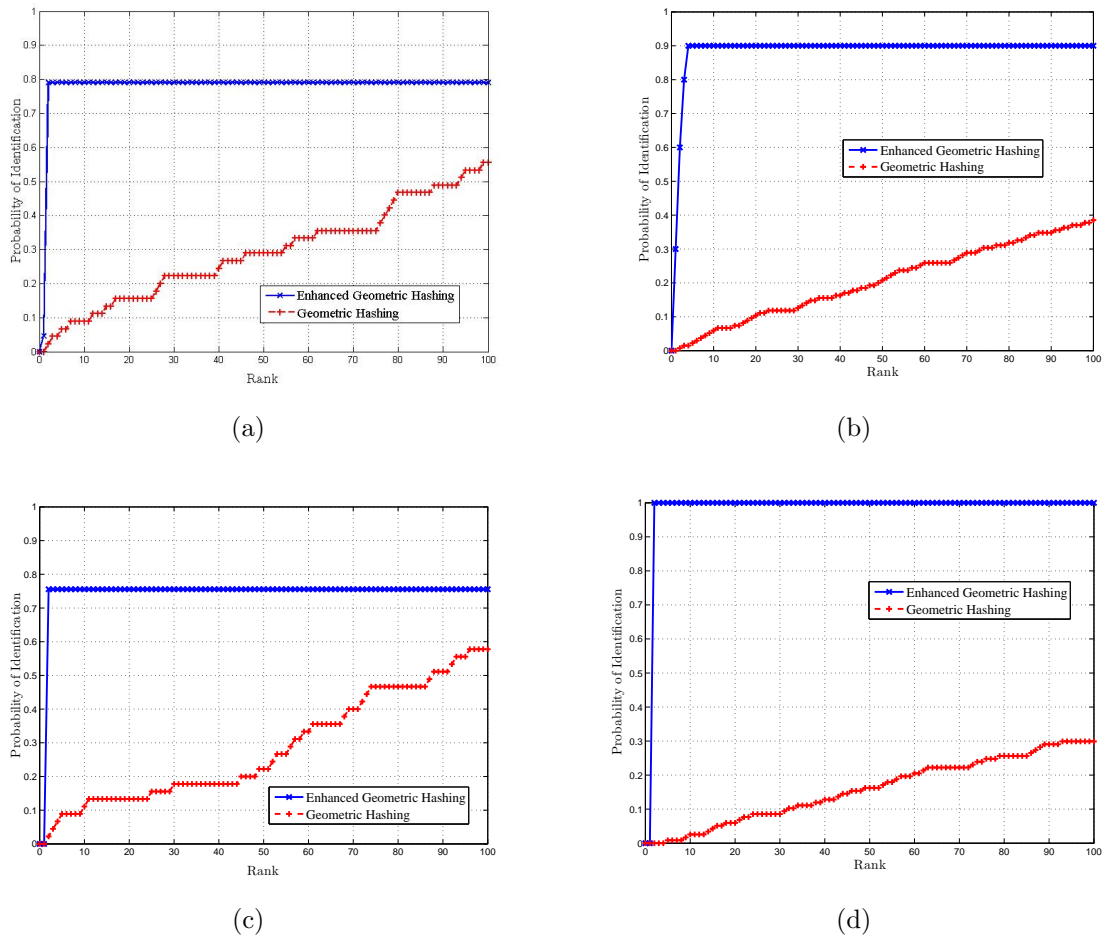


Figure 3.6: CMC curve for geometric hashing and enhanced geometric hashing using SURF on different iris databases, (a) BATH, (b) CASIA, (c) IITK, and (d) UBIRIS.

Experimental results for CASIA and IITK iris databases are shown in Figure 3.6(b) and Figure 3.6(c) respectively. Computation time of enhanced geometric hashing is less than traditional geometric hashing for each database as shown in Table 3.1. Both hashing schemes take more time for CASIA and IITK than BATH and UBIRIS iris databases because computation time depends on the number of keypoints detected by feature extraction technique. Images taken from CASIA and IITK databases show more details than UBIRIS and BATH.

Table 3.3: Identification probabilities at various ranks for geometric hashing (GH) and enhanced geometric hashing (EGH) using SURF keypoints.

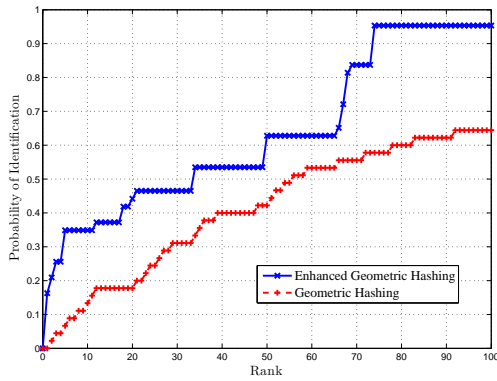
Ranks	UBIRIS		BATH		CASIA		IITK	
	GH	EGH	GH	EGH	GH	EGH	GH	EGH
1	0.0	0.0	0.0	0.0465	0.0	0.3	0.0	0.0
2	0.0	1	0.0222	0.7907	0.0074	0.6	0.0222	0.7556
3	0.0	1	0.0444	0.7907	0.0148	0.8	0.0444	0.7556
5	0.0085	1	0.0667	0.7907	0.0222	0.9	0.08889	0.7556
10	0.0256	1	0.08889	0.7907	0.0592	0.9	0.1111	0.7556
20	0.0598	1	0.1556	0.7907	0.2374	0.9	0.1333	0.7556
30	0.08547	1	0.2222	0.7907	0.1259	0.9	0.1778	0.7556
50	0.1624	1	0.2889	0.7907	0.2074	0.9	0.2222	0.7556
100	0.2991	1	0.5556	0.7907	0.3852	0.9	0.5778	0.7556

3.3.3 Comparative analysis using BRISK

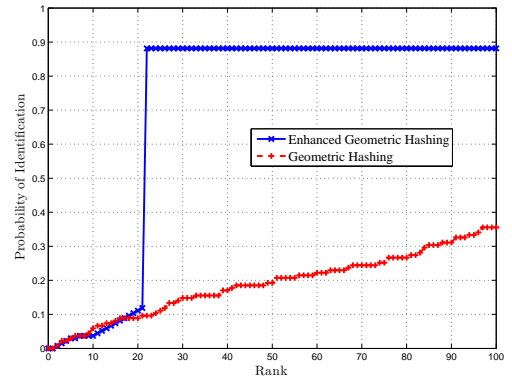
A recently developed keypoint descriptor BRISK is applied with both hashing schemes in a comparative manner. BRISK performs at a dramatically lower computational cost. The main reason of speed is the use of bit-string descriptor. The number of bits different in the two descriptors is a measure of their dissimilarity. The respective operations reduce to a bitwise *XOR* followed by a bit count, which can both be computed very efficiently. Geometric hashing performs with maximum identification probabilities 0.29, 0.64, 0.35, and 0.59 with respect to UBIRIS, BATH, CASIA, and IITK iris datasets respectively. Enhanced geometric hashing achieves maximum identification probabilities 0.58, 0.95, 0.88, and 0.71 with respect to UBIRIS, BATH, CASIA, and IITK iris datasets respectively, by taking top 100 ranks into consideration as shown in Table 3.4. The results show that enhanced geometric hashing is more efficient than traditional geometric hashing. Comparison between geometric hashing and enhanced geometric hashing using BRISK on different iris databases BATH, CASIA, IITK, and UBIRIS are shown in Figure 3.7(a), Figure 3.7(b), Figure 3.7(c), and Figure 3.7(d) respectively.

Table 3.4: Identification probabilities at various ranks for geometric hashing (GH) and enhanced geometric hashing (EGH) using BRISK keypoints.

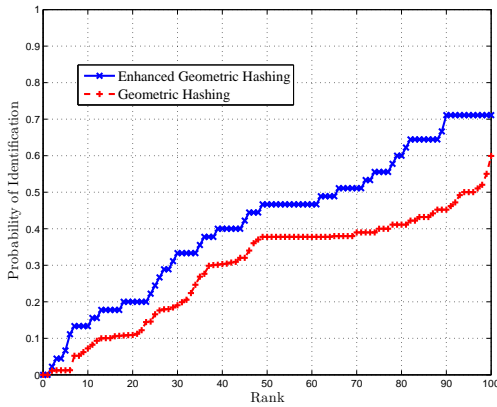
Ranks	UBIRIS		BATH		CASIA		IITK	
	GH	EGH	GH	EGH	GH	EGH	GH	EGH
1	0.0	0.0	0.0	0.1628	0.0	0.0	0.0	0.0
2	0.0	0.0854	0.2222	0.2093	0.007407	0.0074	0.0111	0.0222
3	0.0	0.08547	0.0444	0.2558	0.022	0.02222	0.0111	0.0.444
5	0.0085	0.1111	0.06667	0.3488	0.375	0.03704	0.01243	0.06667
10	0.03419	0.1538	0.1333	0.3488	0.05926	0.05185	0.07223	0.1333
20	0.0854	0.2222	0.1778	0.4419	0.08889	0.1111	0.109	0.2
30	0.1026	0.3248	0.3111	0.4651	0.1481	0.8815	0.1905	0.333
50	0.188	0.3675	0.4222	0.6279	0.1926	0.8815	0.3778	0.4667
100	0.2906	0.5812	0.6444	0.9535	0.3556	0.8815	0.5993	0.7111



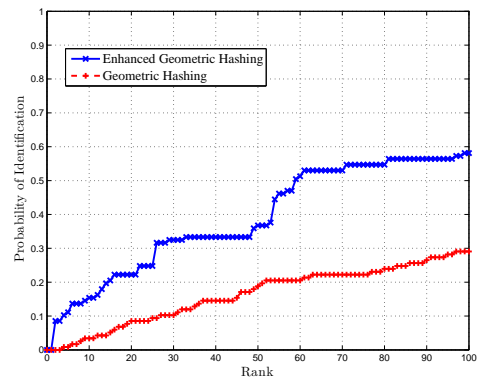
(a)



(b)



(c)



(d)

Figure 3.7: CMC curve for geometric hashing and enhanced geometric hashing using BRISK on different iris databases, (a) BATH, (b) CASIA, (c) IITK, and (d) UBIRIS.

3.4 Summary

Geometric hashing is found to be robust to similarity transformations, occlusion as well as nonuniform illumination. Features are extracted directly from annular iris image to overcome the effect of aliasing. Enhanced geometric hashing effectively removes the use of bases pairs thus reduce the time complexity by a factor of nC_2 . Overhead in the enhanced geometric hashing is the use of PCA, which is negligible. In the enhanced geometric hashing, since each feature point is inserted exactly once, both memory and searching cost has been reduced significantly. From the results obtained from experiments, it is evident that the enhanced geometric hashing is much faster and more accurate than traditional geometric hashing.

Chapter 4

Conclusions and Future Work

This thesis proposes a comparative study of geometric hashing and enhanced geometric hashing schemes, using local feature extraction techniques, for cooperative as well as non-cooperative iris databases. Global approaches fail to work for large variations in individual's pose, illumination, and occlusion. Further, global approaches are not suitable for noise independent annular iris as the size of iris varies due to illumination. Local features are less sensitive to variations since the descriptors are extracted from the neighboring regions around interest points. At first level, geometric hashing with SIFT has been applied to iris for feature extraction and matching. Geometric hashing performs with maximum identification probabilities 0.69, 0.74, 0.48, and 0.80 with respect to UBIRIS, BATH, CASIA, and IITK iris datasets respectively, by taking top 100 ranks. But the main drawback of geometric hashing with SIFT is that both are computationally costly. Enhanced geometric hashing with SIFT performs better than traditional geometric hashing. It achieves maximum identification probabilities 0.79, 0.91, 0.82, and 0.97 with respect to UBIRIS, BATH, CASIA, and IITK iris datasets respectively, by taking top 100 ranks into consideration. At second level, both hashing schemes use SURF as a local feature descriptor. SURF outperforms in comparison to previously proposed keypoint descriptors with respect to repeatability, distinctiveness, robustness, and time. Geometric hashing using SURF keypoints performs with maximum identification probabilities 0.29, 0.55, 0.38, and 0.57 with respect to UBIRIS, BATH, CASIA, and IITK iris datasets respectively, by taking top 100 ranks. Enhanced geometric hashing achieves maximum identification probabilities 1, 0.79, 0.9, and 0.75 with respect to UBIRIS, BATH, CASIA, and IITK iris

datasets respectively, by taking top 100 ranks. At last level, a recently developed keypoint descriptor called BRISK is applied with both hashing schemes in a comparative manner. BRISK performs at a dramatically lower computational cost than previously existing techniques. The main reason of speed is the use of bit-string descriptor. This descriptor is computed from intensity comparisons retrieved by dedicated sampling of each keypoint neighborhood. Geometric hashing with BRISK descriptor performs with maximum identification probabilities 0.29, 0.64, 0.35, and 0.59 with respect to UBIRIS, BATH, CASIA, and IITK iris datasets respectively, by taking top 100 ranks. Enhanced geometric hashing achieves maximum identification probabilities 0.58, 0.95, 0.88, and 0.71 with respect to UBIRIS, BATH, CASIA, and IITK iris datasets respectively, by taking top 100 ranks. The results show that enhanced geometric hashing is more efficient than traditional geometric hashing.

The research findings made out of this thesis has opened several research directions, which have a scope for further investigations. The limitations can be refined that promotes further research in the proposed area. The sector based iris approach used fixed size mask for removing eyelids. This fails for images with no occlusion or occlusion greater than the mask size. Thus, an adaptive mask is required that can automatically detect eyelids by fitting curves on the lower and upper eyelid edge segments. Performance of BRISK with enhanced geometric hashing can be further improved by increasing the number of detected interest points. The computational cost of geometric hashing can be further reduced by using a clustering technique or dimensionality reduction approach. This will reduce the number of basis pairs $\binom{n}{2}$ while still preserving identification accuracy.

Bibliography

- [1] “CASIA Database. <http://www.cbsr.ia.ac.cn/english/IrisDatabase.asp>.”
- [2] H. Mehrotra, “Iris identification using keypoint descriptors and geometric hashing.” M.Tech(Research) dissertation, National Institute of Technology Rourkela (India), 2010.
- [3] H. Mehrotra, B. Majhi, and P. Gupta, “Robust iris indexing scheme using geometric hashing of sift keypoints,” in *Journal of Network and Computer Applications*. Elsevier, 2010, vol. 33, no. 3, pp. 300–313.
- [4] D. G. Lowe, “Distinctive image features from scale-invariant keypoints,” in *International Journal of Computer Vision*. Springer, 2004, vol. 60, no. 2, pp. 91–110.
- [5] H. Bay, T. Tuytelaars, and L. Van Gool, “Surf: Speeded up robust features,” in *European Conference on Computer Vision*. Springer, 2006, pp. 404–417.
- [6] H. Bay, A. Ess, T. Tuytelaars, and L. Van Gool, “Speeded-up robust features (surf),” in *Computer Vision and Image Understanding*. Elsevier, 2008, vol. 110, no. 3, pp. 346–359.
- [7] S. Leutenegger, M. Chli, and R. Y. Siegwart, “Brisk: Binary robust invariant scalable keypoints,” in *International Conference on Computer Vision (ICCV)*. IEEE, 2011, pp. 2548–2555.
- [8] A. K. Jain, R. M. Bolle, and S. Pankanti, “Biometrics: personal identification in networked society.” Springer, 1999.
- [9] A. K. Jain, A. Ross, and S. Prabhakar, “An introduction to biometric recognition,” in *IEEE Transactions on Circuits and Systems for Video Technology*, 2004, vol. 14, no. 1, pp. 4–20.
- [10] A. K. Jain, P. Flynn, and A. A. Ross, “Handbook of biometrics.” Secaucus, NJ, USA: Springer-Verlag New York, Inc., 2007.
- [11] D. Maio and A. K. Jain, “Handbook of fingerprint recognition.” springer, 2009.
- [12] J. L. Wayman, A. K. Jain, D. Maltoni, and D. Maio, “Biometric systems: Technology, design and performance evaluation.” Secaucus, NJ, USA: Springer-Verlag New York, Inc., 2004.
- [13] J. Daugman, “The importance of being random: statistical principles of iris recognition,” in *Pattern recognition*. Elsevier, 2003, vol. 36, no. 2, pp. 279–291.

-
- [14] S. A. Sirohey, A. Rosenfeld, and Z. Duric, “Eye tracking.” Computer Vision Laboratory, Center for Automation Research, University of Maryland, 1999.
- [15] J. L. Wayman, “Error rate equations for the general biometric system,” in *IEEE Robotics & Automation Magazine*, 1999, vol. 6, no. 1, pp. 35–48.
- [16] M. Golfarelli, D. Maio, and D. Maltoni, “On the error-reject trade-off in biometric verification systems,” in *IEEE Transactions on Pattern Analysis and Machine Intelligence*. Washington, DC, USA: IEEE Computer Society, 1997, vol. 19, no. 7, pp. 786–796.
- [17] A. Y. Johnson, J. Sun, and A. F. Bobick, “Predicting Large Population Data Cumulative Match Characteristic Performance from Small Population Data,” in *AVBPA*, 2003, pp. 821–829.
- [18] H. Proença and L. A. Alexandre, “Ubiris: A noisy iris image database,” in *13th International Conference on Image Analysis and Processing - ICIAP*. Springer, 2005, pp. 970–977.
- [19] “BATH University Database. <http://www.bath.ac.uk/elec-eng/research/sipg/irisweb>.”
- [20] “Database of Indian Institute of Technology Kanpur. <http://www.cse.iitk.ac.in/users/biometrics>.”
- [21] R. Wildes, “Iris recognition: an emerging biometric technology,” in *Proceedings of the IEEE*, 1997, vol. 85, no. 9, pp. 1348–1363.
- [22] L. Flom and A. Safir, “Iris recognition system,” U.S. Patent 4,641,349, 1987.
- [23] J. Daugman, “Biometric personal identification system based on iris analysis,” U.S. Patent No. 5,291,560, 1994.
- [24] A. Yuille, D. Cohen, and P. Hallinan, “Feature extraction from faces using deformable templates,” in *IEEE Computer Society Conference on Computer Vision and Pattern Recognition*, 1989, pp. 104–109.
- [25] J. Daugman, “How iris recognition works,” in *International Conference on Image Processing 2002*, 2002, vol. 1, pp. 33–36.
- [26] Z. Sun, T. Tan, and Y. Wang, “Robust encoding of local ordinal measures: A general framework of iris recognition,” in *Biometric Authentication*. Springer, 2004, pp. 270–282.
- [27] P. Yao, J. Li, X. Ye, Z. Zhuang, and B. Li, “Iris recognition algorithm using modified log-gabor filters,” in *Proceedings of the 18th International Conference on Pattern Recognition*, 2006, pp. 461–464.
- [28] D. M. Monro, S. Rakshit, and D. Zhang, “DCT-based Iris Recognition,” in *IEEE Transactions on Pattern Analysis and Machine Intelligence*, 2007, vol. 29, no. 4, pp. 586–595.
- [29] F. Alonso-Fernandez, P. Tome-Gonzalez, V. Ruiz-Albacete, and J. Ortega-Garcia, “Iris recognition based on sift features,” in *International Conference on Biometrics, Identity and Security (BIDS)*. IEEE, 2009, pp. 1–8.

-
- [30] H. J. Wolfson and I. Rigoutsos, "Geometric hashing: An overview," in *Computational Science & Engineering*. IEEE, 1997, vol. 4, no. 4, pp. 10–21.
- [31] A. Mhatre, S. Chikkerur, and V. Govindaraju, "Indexing biometric databases using pyramid technique," in *International Conference on Audio and Video Based Biometric Person Authentication (AVBPA)*, 2005, pp. 841–849.
- [32] N. B. Pusan and N. Sudha, "A novel iris database indexing method using the iris color," in *3rd IEEE Conference on Industrial Electronics and Applications*, 2008, pp. 1886–1891.
- [33] U. Jayaraman, A. K. Gupta, S. Prakash, and P. Gupta, "An enhanced geometric hashing," in *International Conference on Communications (ICC)*. IEEE, 2011, pp. 1–5.
- [34] L. Ma, T. Tan, Y. Wang, and D. Zhang, "Efficient iris recognition by characterizing key local variations," in *Image Processing, IEEE Transactions on*. IEEE, 2004, vol. 13, no. 6, pp. 739–750.
- [35] W. W. Boles and B. Boashash, "A Human Identification Technique using Images of the Iris and Wavelet Transform," in *IEEE Transactions on Signal Processing*, 1998, vol. 46, no. 4, pp. 1185–1188.
- [36] K. Bowyer, K. Hollingsworth, and P. J. Flynn, "Image understanding for iris biometrics: A survey," in *Computer Vision and Image Understanding*, 2008, vol. 110, no. 2, pp. 281–307.
- [37] S. K. Pal and P. Mitra, "Pattern recognition algorithms for data mining: Scalability, knowledge discovery, and soft granular computing." London, UK: Chapman & Hall, Ltd., 2004.
- [38] A. K. Pujari, "Data mining techniques." India: Universities Press, 2001.
- [39] L. V. Birgale and M. Kokare, "Iris recognition using discrete wavelet transform," in *International Conference on Digital Image Processing*. IEEE, 2009, pp. 147–151.
- [40] L. Masek *et al.*, "Recognition of human iris patterns for biometric identification," Ph.D. dissertation, University of Western Australia, 2003.
- [41] E. Rosten and T. Drummond, "Fusing points and lines for high performance tracking," in *Tenth IEEE International Conference on Computer Vision*. IEEE, 2005, vol. 2, pp. 1508–1515.
- [42] "SIFT for Matlab. <http://www.vlfeat.org/~vedaldi/code/sift.html>."
- [43] T. Lindeberg, "Feature detection with automatic scale selection," in *International Journal of Computer Vision*. Hingham, MA, USA: Kluwer Academic Publishers, 1998, vol. 30, no. 2, pp. 79–116.
- [44] K. Mikolajczyk and C. Schmid, "An affine invariant interest point detector," in *Proceedings of the 7th European Conference on Computer Vision-Part I*. Springer-Verlag, 2002, pp. 128–142.

- [45] P. Viola and M. Jones, “Rapid object detection using a boosted cascade of simple features,” in *Proceedings of IEEE Computer Society Conference on Computer Vision and Pattern Recognition*, 2001, vol. 1, pp. 511–518.
- [46] P. S. Eon, P. Y. Simard, P. Haffner, and Y. Lecun, “Boxlets: a fast convolution algorithm for signal processing and neural networks,” in *Advances in Neural Information Processing Systems*. MIT Press, 1999, pp. 571–577.
- [47] Y. Fang, J. Cheng, K. Wang, and H. Lu, “Hand gesture recognition using fast multi-scale analysis,” in *Fourth International Conference on Image and Graphics*, 2007, pp. 694–698.
- [48] M. Brown and D. Lowe, “Invariant features from interest point groups,” in *British Machine Vision Conference*, 2002, pp. 656–665.
- [49] E. Mair, G. D. Hager, D. Burschka, M. Suppa, and G. Hirzinger, “Adaptive and generic corner detection based on the accelerated segment test,” in *European Conference on Computer Vision*. Springer, 2010, pp. 183–196.
- [50] R. Bolle and S. Pankanti, “Biometrics personal identification in networked society.” Norwell, MA, USA: Kluwer Academic Publishers, 1998.
- [51] Y. Lamdan and H. J. Wolfson, “Geometric hashing: A general and efficient model-based recognition scheme,” in *International Conference on Computer Vision (ICCV)*, 1988, vol. 88, pp. 238–249.
- [52] W. Grimson and D. Huttenlocher, “On the sensitivity of geometric hashing,” in *Third International Conference on Computer Vision*, 1990, pp. 334–338.
- [53] H. V. Dijck, “Object recognition with stereo vision and geometric hashing,” Ph.D. dissertation, Advanced School for Computing and Imaging, University of Twente, P.O. Box 217, 7500 AE Enschede, Netherlands, 1999.
- [54] I. Rigoutsos and R. Hummel, “Implementation of geometric hashing on the Connection Machine,” in *Workshop on Directions in Automated CAD-Based Vision*, 1991, pp. 76–84.

Dissemination

1. **Ravi Kumar** and Banshidhar Majhi, "Iris Recognition using BRISK and PCA," *Research Scholars' Day Celebration 2013*, Indian Institute of Space Science and Technology, Thiruvananthapuram, India, December 2013.

Ravi Kumar

Computer Science and Engineering Department,
National Institute of Technology Rourkela,
Rourkela – 769 008, India.

+91 89840 88927.

ravimitharwal@yahoo.com

Qualification

- M.Tech. (Research) (CSE) (Continuing)
National Institute of Technology Rourkela.
- B.E. (CSE)
Maharana Pratap University of Agriculture and Technology, Udaipur, [64.70%]
- 12th
Rajasthan Board of Secondary Education, Ajmer, [75.69%]
- 10th
Rajasthan Board of Secondary Education, Ajmer, [74.33%]

Permanent Address

Village – Kishanpura
Po – Shishu Ranoli
Dist – Sikar
State – Rajasthan Pin – 332 405 (India)

Date of Birth

July 01, 1991